Xu J., Alexander DB., Iigo M., Hamano H., Takahashi S., Yokoyama T., Kato M., Usami I. , Tokuyama T., Tsutsumi M., Tamura M., Oguri T., Niimi A., Hayashi Y., Yokoyama Y.,Tonegawa K., Fukamachi K., Futakuchi M., Sakai Y., Suzui M., Kamijima M., Hisanaga N., Omori T., Hirose A., Kanno J., Nakae D., and Tsuda H	Chemokine (C-C motif) ligand 3 detection in the serum of persons exposed to asbestos: A patient-based study.	Cancer Sci.		in press	2015

Ⅳ．研究成果の刊行物・別冊

Journal of Chromatography B, 988 (2015) 149–156

Contents lists available at ScienceDirect

Journal of Chromatography B

journal homepage: www.elsevier.com/locate/chromb

Comprehensive analysis of the lipophilic reactive carbonyls present in biological specimens by LC/ESI-MS/MS

Susumu Tomono*, Noriyuki Miyoshi, Hiroshi Ohshima

Laboratory of Longevity Biochemistry, Graduate School of Integrated Pharmaceutical and Nutritional Sciences, Graduate Program in Food and Nutritional Sciences, University of Shizuoka, Shizuoka 422-8526, Japan

ARTICLE INFO

Article history:
Received 6 September 2014
Accepted 25 February 2015
Available online 2 March 2015

Keywords:
Reactive carbonyl
Aldehyde
Dansyl hydrazine
LC/ESI-MS/MS
SRM
Lipid peroxidation

ABSTRACT

A new analytical method has been developed for profiling lipophilic reactive carbonyls (RCs) such as aldehydes and ketones in biological samples using liquid chromatography/electrospray ionization tandem mass spectrometry (LC/ESI-MS/MS) with selected reaction monitoring (SRM). The method consists of several phases, including (1) extraction of lipophilic RCs with a chloroform/methanol mixture; (2) derivatization of the extracted RCs with dansyl hydrazine (DH); and (3) SRM detection of the characteristic product ion of the 5-dimethylaminonaphthalene-1-sulfonyl moiety (*m/z* 236.1). The analytical results were expressed as RC maps, which allowed for the occurrence and levels of different lipophilic RCs to be visualized. We also developed a highly reproducible and accurate method to extract, purify and derivatize RCs in small volumes of biological specimens. This method was applied to the detection of free RCs in mice plasma samples, and resulted in the detection of more than 400 RCs in samples obtained from C57BL/6J mice. Thirty-four of these RCs were identified by comparison with authentic RCs. This method could be used to investigate the levels of RCs in biological and environmental samples, as well as studying the role of lipid peroxidation in oxidative stress related-disorders and discovering new biomarkers for the early diagnosis of these diseases.

© 2015 Published by Elsevier B.V.

1. Introduction

A wide variety of aldehydes and ketones (i.e., reactive carbonyls; RCs) can be found in human tissues and the environment, and these compounds are generally formed by the lipid peroxidation (LPO) of phospholipids (PLs), triacylglycerols (TGs), cholesterol and cholesteryl esters. For example, polyunsaturated fatty acids (PUFAs), which can be used to form PLs or TGs, can be oxidized to form lipid hydroperoxides [1], which can subsequently decompose to give a variety of different RCs, including alkanals, alkenals, 4-hydroxyalkenals and alkadienals [2–4]. RCs react with the amino groups in proteins, amino acids, nucleic acids, and PLs such as phosphatidylethanolamine and phosphatidylserine, to give the corresponding Schiff base adducts [4–8]. α,β-Unsaturated aldehydes, in particular, are highly reactive and readily undergo Michael addition reactions with amino and thiol groups to give the corresponding 1,4-addition products [9,10]. Increased levels of RCs such as acrolein, 4-hydroxy-2-nonenal (HNE) and malondialdehyde in human tissues have therefore been associated with elevated risks of cardiovascular disease and cancer, as well as several other chronic diseases, because they can react directly with proteins and nucleic acids and have an adverse impact on their structure, function and overall utility [4,5,11,12]. However, information pertaining to the occurrence and levels of various RCs in complicated biological specimens, as well as our general knowledge and understanding of their roles in diseases, remains limited.

A broad range of different analytical methods has been reported for investigating RCs. For example, the physiological and pathological levels of RCs can be analyzed by GC/MS following the conversion of the RCs to the corresponding *O*-pentafluorobenzyl-oxime (PFB-oxime) derivatives, and the subsequent conversion of the hydroxy moieties in the resulting oximes to the trimethylsilyl (TMS) ether derivatives [13]. 2,4-Dinitrophenylhydrazine (DNPH) has also been used to derivatize the RCs present in a variety of biological and environmental samples. The DNPH derivatives can be analyzed by HPLC

Abbreviations: AA, arachidonic acid; DH, dansyl hydrazine; DHA, docosahexaenoic acid; 2,4-DDE, 2,4-decadienal; EDE, 4,5-epoxy-2-decenal; 2,4-HxDE, 2,4-hexadienal; 2,4-HpDE, 2,4-heptadienal; HNE, 4-hydroxy-2-nonenal; IS, internal standard; LA, linoleic acid; LC/ESI-MS/MS, liquid chromatography/electrospray ionization tandem mass spectrometry; LPO, lipid peroxidation; 2,4-NDE, 2,4-nonadienal; ONE, 4-oxo-2-nonenal; PLs, phospholipids; PUFAs, polyunsaturated fatty acids; RCs, reactive carbonyls; RSD, relative standard deviation; SRM, selected reaction monitoring; TGs, triacylglycerols.

* Corresponding author. Tel.: +81 54 264 5531; fax: +81 54 264 5530.
E-mail address: gp1535@u-shizuoka-ken.ac.jp (S. Tomono).

http://dx.doi.org/10.1016/j.jchromb.2015.02.036
1570-0232/© 2015 Published by Elsevier B.V.

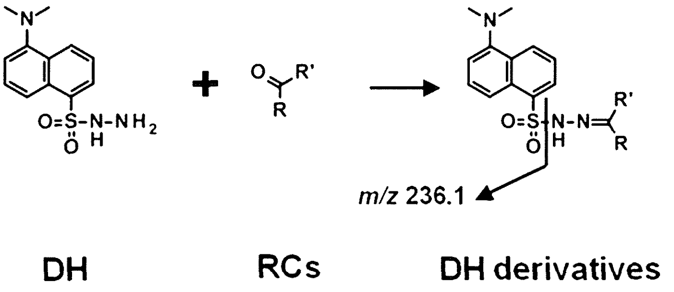

Fig. 1. Chemical structures of the RCs derivatized with DH, and the product ion with an m/z value of 236.1 formed by CID.

with UV detection or LC/MS [14,15]. Unfortunately, however, these methods lack the sensitivity and specificity required for the comprehensive analysis of trace amounts of the different RCs present in complicated biological and environmental samples.

Dansyl hydrazine (DH) is a fluorescent derivatization reagent that has been used for fluorescence detection as well as enhancing the ionization characteristics of aldehydes and ketones [16–18]. There are several advantages associated with the use of DH over other derivatizing agents. Most notably, the dimethylamino group of DH can be readily protonated under acidic conditions [19], and the resulting positively ionized DH derivatives can generate a product ion with an m/z value of 236.1 by collision-induced dissociation (CID). The detection of a product ion with an m/z value of 236.1 is therefore consistent with the formation of a 5-dimethylaminonaphthalene-1-sulfonyl moiety from the cleavage of the parent DH derivative (Fig. 1). Furthermore, the product ion spectra of the DH derivatives of RCs are generally simple and clear.

The aim of the current study was to develop a sensitive and specific method for the simultaneous detection of numerous lipophilic RCs using DH as a derivatizing agent. Verification experiments revealed that the product ion for the 5-dimethylaminonaphthalene-1-sulfonyl moiety (m/z 236.1) generated from the positively ionized RC-DH derivatives during the CID process could be measured over specific transition ranges. In this way, the mass spectral data could be used to provide unique signatures for the different RCs present in biological samples. The presence and quantity of various RCs in the different samples could then be compared by creating “RC maps” that consisted of the LC/MS retention times, m/z values, and relative peak intensities of the potential RCs. This approach allowed for the comprehensive detection of a variety of different RCs over a wide range of molecular weights, including those with unknown structures. Furthermore, this method was found to be highly sensitive and repeatable for the measurement of a range of RCs, as well as being applicable to different biological and environmental samples. This newly developed method was also validated for the quantification of free RCs present in the plasma of C57BL/6J mice.

2. Material and methods

2.1. Materials

Dansyl hydrazine (DH) was purchased from Invitrogen (Carlsbad, CA, USA). *p*-Toluenesulfonic acid (*p*-TsOH) and the RCs, including propanal, pentanal, butanal, 2-hexenal, hexanal, 2-heptenal, heptanal, octanal, 2-nonenal, nonanal, decanal, undecanal, dodecanal and tridecanal, were obtained from Sigma–Aldrich (St. Louis, MO, USA). Glyoxal, crotonaldehyde, 2,4-nonadienal (NDE), 2,4-decadienal (DDE), heptadecanal, hexadecanal, octadecanal, pentadecanal and tetradecanal were purchased from Tokyo Chemical Industry (Tokyo, Japan). 4-Hydroxy-2-hexenal (HHE), 4-hydroxy-2-nonenal (HNE), 4-oxo-2-nonenal (ONE) and 4,5-epoxy-2-decenal (EDE) were purchased from Cayman Chemical Company (Ann Arbor, MI, USA). *p*-Benzyloxybenzaldehyde (*p*-BOBA) and all of the other chemicals used in the current study were purchased from Wako Pure Chemical Industries (Osaka, Japan). Secosterols A and B were synthesized according to the procedure reported by Wentworth et al. [20], and their purities were verified by TLC and ^{1}H NMR analyses. Stock solutions of the RCs and an internal standard (IS) (*p*-BOBA 10 μM) were prepared separately in acetonitrile and stored at −20 °C prior to their use.

2.2. Profiling of the RCs in plasma

Frozen mouse plasma samples (stored −80 °C) were thawed on ice to 0 °C. Immediately after being thawed, a portion of the plasma sample (20 μL) was added to a solution consisting of 80 μL of distilled water, 2 μL of 10 μM IS (*p*-BOBA) and 200 μL of a mixture of chloroform/methanol (2:1, v/v), and the resulting mixture was vigorously agitated for 1 min. The mixture was then centrifuged at 15,000 rpm for 10 min and the organic phase was collected. The remaining precipitate and aqueous phase were then mixed with 200 μL of a mixture of chloroform/methanol (2:1, v/v), and the resulting mixture was centrifuged at 15,000 rpm for 10 min to give the organic phase. The combined organic phases were then subjected to a derivatization reaction with DH according to the procedure described below.

2.3. DH derivatization

The samples were mixed with 100 μL of acetonitrile containing 50 μg of DH and 10 μg of *p*-TsOH, and the resulting mixtures were incubated for 4 h at ambient temperature in the absence of light. The mixtures were then evaporated to dryness in vacuo to give the corresponding derivatized residues, which were individually dissolved in 200 μL of acetonitrile. Aliquots (5 μL) of these stock solutions were analyzed seven times by LC/ESI-MS/MS as described below.

2.4. LC/ESI-MS/MS

The LC/ESI-MS/MS analyses were performed on an Agilent 1200 series HPLC system (Agilent Technologies, Santa Clara, CA, USA) using a TSKgel Super-Octyl column (2.3 μm, 100 mm × 2.0 mm, TOSOH, Tokyo, Japan) and an Agilent G6410B triple quadrupole tandem mass spectrometer with an electrospray ionization device running in the positive ion mode. The detector conditions were as follows: capillary voltage at 4000 V, source temperature of 300 °C, drying gas flow rate of 7 L/min, nebulizer gas at 20 psi, fragmentor at 200 V and collision energies of 13 eV (m/z 275–349), 20 eV (m/z 350–449) and 29 eV (m/z 450–949). Nitrogen was used as the collision gas. The RC-DH derivatives were detected using the selected reaction monitoring (SRM) mode. This strategy was designed to detect a specific product ion with an m/z value of 236.1 by CID. This product ion was assigned to the 5-dimethylaminonaphthalene-1-sulfonyl moiety derived from the positively ionized DH derivatives. The RC-DH derivatives were therefore detected with high sensitivity by monitoring their transmitting $[M+H]^+ \rightarrow 236.1$ transitions (Fig. 1). A total of 675 SRM transitions were monitored for each DH-derivatized sample, with the transitions ranging from m/z 275 → 236.1 to 949 → 236.1, and a total of 100 channels were monitored simultaneously for each sample injection. One channel from each injection was reserved for monitoring the transition of *p*-BOBA-DH (IS) at m/z 460 → 236.1. Each sample was injected seven times to complete the monitoring of the 675 SRM transitions.

In order to verify whether the peaks of DH-derivatives were derived from aldehydes, ketones or other artifacts, mixtures of standard RCs or mice plasma samples were reduced by treatment for 1 h at 37 °C with 0.1 M sodium borohydride ($NaBH_4$). $NaBH_4$ can convert aldehydes and ketones to corresponding primary and secondary alcohols, which are not derivatized with DH. After the reduction of standard RCs or mice plasma samples with $NaBH_4$, the peaks corresponding to DH-RCs were not detected by LC/ESI-MS/MS (SRM) except for those which were derived from DH reagents (data not shown). Some of the solvents used in this study were found to be contaminated with RCs. Therefore, it was necessary to calculate the amounts of RCs by subtracting the redundant (background) peaks such as the spike noises and artifactual DH derivatives derived from solvents and reagents.

In terms of the mobile phases used for the LC/ESI-MS/MS analyses, solvent A consisted of a 0.1% (v/v) solution of formic acid in water, whereas solvent B consisted of a 0.1% (v/v) solution of formic acid in acetonitrile. The DH derivatives were eluted from the column using a linear gradient, which started at 80% solvent A and 20% solvent B, and progressed to 100% solvent B over a period of 10 min. The system was then eluted with 100% solvent B for 10 min before being returned to the initial conditions over a period of 10 min to allow for the equilibration of the column. The system was operated at a constant flow rate of 0.2 mL/min for all of the analyses.

2.5. Stabilities of RCs during storage

Plasma samples were obtained from five 10-week-old male C57BL/6J mice (body weight ~27 g). The plasma samples (100 μL) were spiked with five representative RCs, including 4-hydroxy-2-alkenal (HNE), 2-alkenal (2-hexenal) and 2,4-alkadienal (2,4-NDE), as well as a short chain alkanal (hexanal) (5 pmol each) and a long chain alkanal (hexadecanal) (100 pmol). The spiked samples were then stored on ice for 0–60 min or stored at −80 °C for 4 weeks.

2.6. LOD and LOQ

The limit of detection (LOD) was defined as the calculated concentration at a signal to noise ratio of ≥5 (S/N = 5). The limit of quantification (LOQ) was based on a signal to noise ratio of ≥10 and validated at a concentration measured with an RSD ≤20%.

2.7. Recovery

The plasma samples (20 μL) were spiked or left unspiked (control) with a mixture containing several RC standards at 2 or 10 pmol. The samples were then extracted with a chloroform/methanol (2:1, v/v) mixture and the organic phases were analyzed according to the procedure described above. The estimated recoveries were calculated as follows:

Recovery = [(concentrations of extracted total RCs − concentrations of extracted endogenous RCs)/concentrations of spiked RCs standards] × 100 (%)

2.8. Calibration curves for RCs

Calibration and validation studies were conducted involving the addition of several different RCs to the mice plasma. Varying amounts of the RCs (i.e., 0.1, 0.2, 0.5, 1, 2, 5, 10, 20, 50 and 100 pmol for each RC species) and a fixed amount of the IS (20 pmol) were spiked into the mouse plasma (20 μL), and the resulting mixtures were extracted, derivatized and subjected to LC/ESI-MS/MS analysis. Calibration curves were constructed by plotting the peak area ratios [i.e., (total RCs – endogenous RCs)/IS against the concentration of RCs]. All of the determinations at the different concentrations were performed in triplicate.

2.9. Assay precision and accuracy (analytical recovery)

The accuracy and precision levels of the assay were determined based on intra- and inter-day variations in the results obtained using the method described above.

Plasma samples (20 μL) were spiked with RCs at concentrations of 0, 50, 100, 500 and 1000 pmol/mL, respectively, $n = 3$. IS (20 pmol) was then added to each sample, and the resulting mixtures were extracted, derivatized and analyzed by LC/ESI-MS/MS. The intra-day precision values for the different concentrations were also calculated from determination experiments, which were conducted in triplicate. The inter-day precision was evaluated by analyzing the same sample over a 5-day period, and the precision was determined as the relative standard deviation (RSD, %). The accuracies (analytical recoveries) of the RCs were defined as the total concentration of RCs in the spiked samples/(the concentration of RCs detected in the unspiked samples + the spiked concentration) × 100 (%).

3. Results and discussion

3.1. RCs derivatization with DH

We initially derivatized 36 authentic RCs with DH and analyzed the resulting products by LC/ESI-MS/MS. All of the derivatized RCs gave the corresponding $[M+H]^+$ mass ions, as well as the common product ion with an m/z value of 236.1, which was assigned to the 5-dimethylaminonaphthalene-1-sulfonyl moiety generated from the cleavage of the DH derivatives during CID (Fig. 1). On the basis of these results, we developed a global analytical method for the comprehensive profiling of the lipophilic RCs present in biological samples using LC/ESI-MS/MS with SRM. The SRM assay was designed to detect the characteristic product ion with an m/z value of 236.1, which was derived from the positively ionized RC-DH derivatives transmitting the $[M+H]^+ \rightarrow 236.1$ transition over 675 SRM transitions, ranging from transitions of m/z 275 → 236.1 to 949 → 236.1. For each sample injection, a total of 100 channels were monitored simultaneously. We compared the sensitivities (S/N ratio) of LC/MS detection by SRM and precursor ion scan (PIS) of DH-RC standards (Supplementary Table 1). The sensitivities of SRM were 1.6- to 110-fold better than the PIS. These results indicate that the SRM can be used for the sensitive detection of various RCs by MS.

Supplementary Table 1 can be found, in the online version, at http://dx.doi.org/10.1016/j.jchromb.2015.02.036.

Typical SRM chromatograms for the DH-derivatives of the 36 RCs and IS (*p*-BOBA) are shown in Fig. 2. These results effectively confirmed that the developed SRM assay could be used detect all of the RCs tested in the current study, with the RCs giving the corresponding $[M+H]^+$ ions as well as the common product ion of the 5-dimethylaminonaphthalene-1-sulfonyl moiety by CID. Although 4-hydroxy-2-alkenals such as HNE and HHE possess a chiral center at their C4 position, the *syn*- and *anti*-isomers of their DH derivatives could not be separated in this condition, and it was therefore not possible to detect the different isomers as single peaks. Furthermore, despite using an excess of DH, dicarbonyl compounds such as glyoxal and ONE only reacted to give the mono-DH derivatives under the current derivatization conditions. Ions corresponding to bis-DH derivatives were therefore not observed under these SRM conditions (data not shown).

3.2. Validation of the proposed method using biological samples

This method was validated based on the recovery data and calibration curves of the different RCs that had been spiked into the

Table 1
Linearity, limit of detection (LOD), limit of quantification (LOQ) and recovery values of the LC/ESI-MS/MS assay for the RCs.

Compounds	MW (intact)	$[M+H]^+$ (DH derivatives)	t_R (min)	LOD (fmol)[a]	LOQ (fmol)[b]	Calibration range (fmol)	Linear equation	Linearity (r^2)	Recovery (%)[c]
p-BOBA (IS)	212.21	460	11.8	1	1	–	–	–	101.4
Acrolein	56.06	304	9.3	1	2.5	25–1000	$y = 0.0004x + 0.0052$	0.9996	95.5
Glyoxal	58.04	306	8.4	20	50	50–2500	$y = 0.0014x + 0.0872$	0.9991	100.3[d]
Propanal	58.08	306	9.3	10	25	25–1000	$y = 0.0008x - 0.0043$	0.9978	70.3
Crotonaldehyde	70.09	318	9.8	1	2.5	5–250	$y = 0.0018x + 0.0015$	0.9996	93.8
Butanal	72.11	320	10.1	1	2.5	25–1000	$y = 0.0008x + 0.0245$	0.992	88.4
Pentanal	86.13	334	10.8	10	25	25–1000	$y = 0.0012x + 0.0107$	0.9986	86.0
2,4-HxDE	96.14	344	10.8	1	2.5	5–250	$y = 0.0024x + 0.0224$	0.9944	82.1
2-Hexenal	98.14	346	11.1	1	2.5	5–250	$y = 0.0027x - 0.002$	0.9999	91.4
Hexanal	100.16	348	11.3	10	25	25–1000	$y = 0.0024x + 0.0211$	0.999	93.5
2,4-HpDE	110.17	358	11.2	1	2.5	5–250	$y = 0.0021x + 0.015$	0.995	83.6
2-Heptenal	112.17	360	11.6	1	2.5	5–250	$y = 0.0003x - 0.0009$	0.9997	89.8
HHE	114.14	362	8.9	1	2.5	5–250	$y = 0.0008x - 0.0021$	0.9998	92.5
Heptanal	114.18	362	11.8	10	25	25–1000	$y = 0.0022x + 0.0059$	0.9996	82.5
2-Octenal	126.2	374	12.0	1	2.5	5–250	$y = 0.0139x + 0.103$	0.9952	94.2
Octanal	128.21	376	12.2	10	25	50–2500	$y = 0.0034x - 0.1748$	0.9994	111.8[d]
2,4-NDE	138.22	386	12.1	1	2.5	5–250	$y = 0.0041x + 0.0259$	0.9962	73.6
2-Nonenal	140.22	388	12.4	1	2.5	5–250	$y\text{-}0.0046x - 0.0051$	1	89.6
Nonanal	142.24	390	12.6	20	50	50–2500	$y = 0.0028x - 0.3148$	0.9977	89.0[d]
2,4-DDE	152.21	400	12.5	1	2.5	5–250	$y = 0.0032x + 0.0225$	0.9951	84.6
HNE	156.22	404	10.8	1	2.5	5–250	$y = 0.0006x - 0.0029$	0.9999	93.7
Decanal	156.27	404	13.0	20	50	50–2500	$y = 0.004x - 0.8092$	0.9971	94.6[d]
EDE	168.23	416	11.3	1	2.5	5–250	$y = 0.0023x - 0.0075$	0.9998	86.6
2-Undecenal	168.28	416	13.1	1	2.5	5–250	$y = 0.0153x + 0.0599$	0.9932	88.9
Undecanal	170.29	418	13.3	10	25	25–1000	$y = 0.0004x - 0.1044$	0.9986	92.0
Dodecanal	184.32	432	13.6	20	50	50–2500	$y = 0.0039x - 0.0099$	0.9983	83.2[d]
Tridecanal	198.34	446	13.9	10	25	25–1000	$y = 0.0025x - 0.0013$	0.9995	76.6
Tetradecanal	212.37	460	14.3	10	25	50–2500	$y = 0.0055x - 0.1422$	0.9989	81.2[d]
Pentadecanal	226.4	474	14.6	10	25	25–1000	$y = 0.0013x + 0.0051$	0.9997	84.8
Hexadecanal	240.43	488	14.8	10	25	50–2500	$y = 0.0029x + 0.0112$	0.9999	82.8[d]
Heptadecanal	254.45	502	15.1	1	2.5	5–250	$y = 0.002x - 0.0056$	0.9982	85.7
Octadecanal	268.48	516	15.4	10	25	50–2500	$y = 0.0012x + 0.074$	0.9964	80.1[d]
Secosterol-A	418.34	666	14.4	1	2.5	5–250	$y = 0.0008x - 0.0006$	0.9994	99.3
Secosterol-B	418.34	666	14.8	1	2.5	5–250	$y = 0.0002x - 0.0002$	0.9998	77.3

[a] These values were estimated at a S/N ratio of 5.
[b] These values were estimated at a S/N ratio of 10.
[c] $n = 5$, spiked 2 pmol or [d] 10 pmol.

C57BL/6J mice plasma samples (Table 1). Overall, this method was found to be sensitive, reproducible, accurate and specific for the RCs tested in the current study.

The stability properties of the some typical RCs (i.e., 2-hexenal, hexanal, 2,4-NDE, HNE and hexadecanal) that had been added to the mice plasma were determined experimentally (Fig. 3A, B, Supplementary Fig. 1). Samples of the mouse plasma were spiked with 5 or 100 pmol of specific RCs, and the resulting mixtures were kept on ice for 60 min. Subsequent analysis revealed that almost all of the α,β-unsaturated RCs tested (i.e., 2-hexenal and HNE) disappeared rapidly, whereas the other RCs tested (i.e., hexanal, 2,4-NDE and hexadecanal) disappeared at a much slower rate, with about half of the amounts added remained after an incubation period of 60 min on ice (Fig. 3A). On the other hand, Fig. 3B shows that there were no significant differences between the recoveries of the RCs added to the mouse plasma before and after the samples had been stored 4 weeks at −80 °C. These results suggest that it is necessary to extract the RCs as quickly as possible following thawing of frozen plasma samples to obtain their high recoveries. In addition, in order to analyze unstable aldehydes more accurately, new methods, for example adding stable isotope-labeled aldehydes as IS immediately after sampling, may be further developed and validated. The RCs appeared to react with glutathione or the amino groups of the proteins, amino acids, nucleic acids, and PLs, such as phosphatidylethanolamine and phosphatidylserine, to give the corresponding Schiff base adducts [4–8]. α,β-Unsaturated aldehydes, in particular, are highly reactive and readily undergo Michael addition reactions with amino and thiol groups to give the corresponding 1,4-addition products [9,10]. Compounds of this type can also be metabolized enzymatically into other compounds. For these reasons, in order to evaluate the occurrence and biological reactivities of α,β-unsaturated aldehydes, methods to analyze their adducts with amino acids, proteins, DNA and PLs in biological samples should be further developed.

Supplementary Fig. 1 can be found, in the online version, at http://dx.doi.org/10.1016/j.jchromb.2015.02.036.

Based on the stability results of five representative RCs (Fig. 3A), we proceeded to evaluate the recoveries of several standard RCs that had been added to mouse plasma samples. The recoveries of the RCs tested in the current study were in the range of 70.3–111.8% (Table 1). The corresponding calibration curves, which were obtained by plotting the peak area ratios of the 33 different RCs tested in the current study (tests were conducted at six different concentrations in the range of 2.5–2500 fmol) relative to IS exhibited good linearities ($r^2 > 0.9964$) (Table 1). The LOD values (S/N = 5) were found to be in the range of 1–20 fmol, and the LOQ values (S/N = 10) were in the range of 1–50 fmol on column. The assay precision was examined using mouse plasma samples spiked with two different concentrations of the RCs (Table 2). The RSD values were found to be <19.3% for the intra- and inter-day precision measurements, and the accuracy rates ranged from 75.4 to 119.9% (Table 2). These results effectively indicated that the current method is highly accurate and reproducible. Furthermore, the good linearity, sensitivity, recovery and precision properties of this method suggested that it could be used for the analysis of other human and animal tissue samples.

RCs are organic compounds that are widespread in biological samples. Compounds of this type can be formed from fatty acids,

Table 2
Accuracy (analytical recoveries) and precision of the assay used for the determination of the RCs in mice plasma.

Compound		Added (pmol/mL)	Measured (pmol/mL)[a]	RSD (%)	Accuracy (%)	Compound		Added (pmol/mL)	Measured (pmol/mL)[a]	RSD (%)	Accuracy (%)
Acrolein	Intra-day	–	146.5 ± 13.0	8.9	–	Nonanal	Intra-day	–	652.0 ± 7.9	1.2	–
		100	235.2 ± 20.5	8.7	88.7			500	1073.9 ± 59.5	5.5	84.4
		500	680.4 ± 36.2	5.3	106.8			1000	1518.8 ± 18.4	1.2	86.7
	Inter-day	–	153.6 ± 26.3	17.1	–		Inter-day	–	653.6 ± 27.1	4.1	–
Glyoxal	Intra-day	–	52.0 ± 1.3	2.4	–	2,4-DDE	Intra-day	–	9.4 ± 1.1	11.8	–
		50	108.3 ± 4.2	3.9	112.8			50	64.9 ± 1.2	1.8	110.1
		100	158.1 ± 4.4	2.8	106.1			100	110.1 ± 3.3	3.0	100.7
	Inter-day	–	56.3 ± 3.0	5.3	–		Inter-day	–	9.2 ± 1.1	12.3	–
Propanal	Intra-day	–	58.3 ± 3.8	6.5	–	HNE	Intra-day	–	16.8 ± 1.0	6.1	–
		50	178.2 ± 2.9	1.6	119.9			50	68.2 ± 1.5	2.3	102.7
		100	291.1 ± 1.4	0.5	116.4			100	120.8 ± 2.0	1.6	104.0
	Inter-day	–	59.7 ± 4.0	6.8	–		Inter-day	–	16.6 ± 0.4	2.4	–
Crotonaldehyde	Intra-day	–	14.8 ± 1.7	11.4	–	Decanal	Intra-day	–	493.0 ± 24.6	5.0	–
		50	68.1 ± 1.3	1.9	106.6			500	869.9 ± 36.1	4.1	75.4
		100	118.3 ± 0.6	0.5	103.5			1000	1442.4 ± 30.1	2.1	94.9
	Inter-day	–	15.4 ± 1.8	11.6	–		Inter-day	–	492.2 ± 35.2	7.2	–
Butanal	Intra-day	–	101.4 ± 10.5	10.3	–	EDE	Intra-day	–	1.7 ± 0.1	3.9	–
		100	202.1 ± 10.0	5.0	100.7			50	49.2 ± 0.6	1.2	95.0
		500	605.5 ± 78.8	13.0	100.8			100	103.0 ± 3.2	3.1	101.1
	Inter-day	–	97.0 ± 16.0	16.5	–		Inter-day	–	1.7 ± 0.1	3.9	–
Pentanal	Intra-day	–	65.0 ± 8.1	12.4	–	2-Undecenal	Intra-day	–	4.3 ± 0.5	11.5	–
		50	121.0 ± 13.5	11.2	112.0			50	57.1 ± 1.8	3.2	105.8
		100	155.9 ± 8.6	5.5	90.9			100	105.6 ± 2.5	2.4	101.4
	Inter-day	–	66.8 ± 6.6	9.9	–		Inter-day	–	1.7 ± 0.5	15.9	–
2-HxDE	Intra-day	–	<LOQ	–	–	Undecanal	Intra-day	–	106.3 ± 9.1	8.5	–
		50	53.0 ± 5.7	10.8	105.9			100	189.0 ± 7.4	3.9	82.7
		100	102.0 ± 4.3	4.2	102.0			500	622.0 ± 6.7	1.1	103.1
	Inter-day	–	<LOQ	–	–		Inter-day	–	105.6 ± 7.6	7.6	–
2-Hexenal	Intra-day	–	4.4 ± 0.4	9.0	–	Dodecanal	Intra-day	–	740.5 ± 44.6	6.0	–
		50	53.8 ± 1.6	3.0	98.7			500	1209.6 ± 21.5	1.8	93.8
		100	108.1 ± 1.6	1.5	103.7			1000	1622.8 ± 45.1	2.8	88.2
	Inter-day	–	4.6 ± 0.4	8.4	–		Inter-day	–	745.1 ± 42.6	5.7	–
Hexanal	Intra-day	–	60.0 ± 3.2	5.3	–	Tridecanal	Intra-day	–	151.0 ± 5.0	3.0	–
		50	119.9 ± 23.2	19.3	119.7			100	237.8 ± 6.2	2.6	86.8
		100	155.1 ± 13.9	9.0	95.1			500	631.4 ± 10.4	1.7	96.1
	Inter-day	–	58.7 ± 5.7	9.7	–		Inter-day	–	146.7 ± 7.0	4.7	–
2-HpDE	Intra-day	–	4.7 ± 0.8	16.9	–	Tetradecanal	Intra-day	–	174.3 ± 18.6	10.7	–
		50	59.6 ± 4.0	6.7	109.8			100	272.1 ± 20.5	7.5	97.8
		100	106.0 ± 7.1	6.7	101.3			500	708.9 ± 12.1	1.7	106.9
	Inter-day	–	5.5 ± 0.6	10.3	–		Inter-day	–	177.5 ± 8.4	4.7	–
2-Heptenal	Intra-day	–	5.1 ± 0.4	7.1	–	Pentadecanal	Intra-day	–	188.7 ± 12.8	6.8	–
		50	56.5 ± 0.7	1.2	102.9			100	280.1 ± 23.5	8.4	91.4
		100	106.6 ± 4.1	3.8	101.5			500	664.9 ± 20.7	3.1	95.3
	Inter-day	–	4.8 ± 0.2	3.5	–		Inter-day	–	186.4 ± 13.3	7.1	–
HHE	Intra-day	–	7.1 ± 0.5	6.5	–	Hexadecanal	Intra-day	–	630.8 ± 43.6	6.9	–
		50	57.9 ± 2.6	4.5	101.5			500	1110.9 ± 29.8	2.7	96.0
		100	107.9 ± 4.3	4.0	100.8			1000	1521.3 ± 42.0	2.8	89.1
	Inter-day	–	7.0 ± 0.1	1.6	–		Inter-day	–	634.5 ± 42.8	6.7	–
Heptanal	Intra-day	–	55.1 ± 4.2	7.5	–	Heptadecanal	Intra-day	–	31.2 ± 3.7	11.9	–
		50	102.2 ± 9.0	8.8	94.2			50	84.9 ± 6.7	7.9	107.3
		100	149.9 ± 6.2	4.2	94.9			100	131.2 ± 10.1	7.7	100.0
	Inter-day	–	55.7 ± 6.7	11.9	–		Inter-day	–	31.0 ± 3.3	10.6	–
2-Octenal	Intra-day	–	9.0 ± 0.7	8.1	–	Octadecanal	Intra-day	–	300.8 ± 28.1	9.3	–
		50	58.9 ± 3.2	5.4	99.9			500	729.6 ± 17.1	2.3	85.8
		100	101.3 ± 4.3	4.2	92.3			1000	1113.5 ± 26.9	2.4	81.3
	Inter-day	–	8.9 ± 1.5	16.5	–		Inter-day	–	302.5 ± 27.5	9.1	–
Octanal	Intra-day	–	134.7 ± 11.0	8.1	–	Secosterol-A	Intra-day	–	2.3 ± 0.2	7.4	–
		100	218.9 ± 6.0	2.8	84.8			50	48.4 ± 1.3	2.8	92.1
		500	624.6 ± 21.8	3.5	98.0			100	95.3 ± 6.7	7.1	93.0
	Inter-day	–	132.5 ± 13.4	10.1	–		Inter-day	–	2.3 ± 0.1	2.5	–
2,4-NDE	Intra-day	–	3.8 ± 0.2	5.8	–	Secosterol-B	Intra-day	–	5.9 ± 0.4	6.1	–
		50	52.6 ± 2.8	5.3	97.5			50	49.7 ± 2.5	4.9	87.6
		100	103.1 ± 3.2	3.1	99.2			100	99.4 ± 2.9	2.9	93.5
	Inter-day	–	3.8 ± 0.2	6.0	–		Inter-day	–	5.7 ± 0.2	3.8	–
2-Nonenal	Intra-day	–	20.2 ± 1.7	8.6	–						
		50	67.5 ± 1.4	2.1	94.6						
		100	116.7 ± 3.4	3.0	96.4						
	Inter-day	–	20.2 ± 1.4	6.9	–						

[a] $n = 3$.

amino acids, and aromatic compounds, as well as several other compound classes. The results of a growing number of studies have suggested that RCs could be involved in the development of oxidative stress related disorders, such as cancer, cardiovascular disease, neurodegenerative disease and diabetes, as well as several other diseases associated with aging. Our newly developed method would allow for the exploration of different RCs regardless of their chemical structure, and represents a particularly powerful

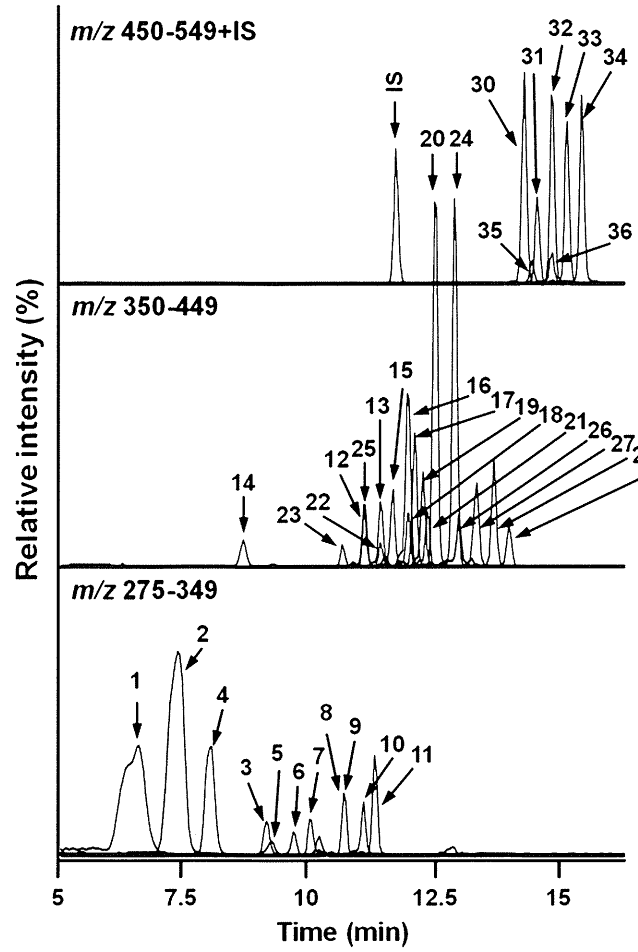

Fig. 2. LC/ESI-MS/MS (SRM) chromatogram of a standard mixture of the RC-DH derivatives (0.5 pmol each). The SRM assay detected the characteristic product ion of the 5-dimethylaminonaphthalene-1-sulfonyl moiety (m/z 236.1), which was derived from the positively ionized RC-DH derivatives transmitting the $[M+H]^+ \rightarrow 236.1$ transition. The peak numbers indicate the names of the RCs as follows: (1) formaldehyde (t_R:7.5 min, m/z 278); (2) acetaldehyde (t_R:7.5 min, m/z 292); (3) acrolein (t_R:9.3 min, m/z 304); (4) glyoxal (t_R:8.4 min, m/z 306); (5) propanal (t_R:9.3 min, m/z 306); (6) crotonaldehyde (t_R:9.8 min, m/z 318); (7) butanal (t_R:10.1 min, m/z 320); (8) pentanal (t_R:10.8 min, m/z 334); (9) 2,4-HxDE (t_R:10.8 min, m/z 344); (10) 2-hexenal (t_R:11.1 min, m/z 346); (11) hexanal (t_R:11.3 min, m/z 348); (12) 2,4-HpDE (t_R:11.2 min, m/z 358); (13) 2-heptenal (t_R:11.6 min, m/z 360); (14) HHE (t_R:8.9 min, m/z 362); (15) heptanal (t_R:11.8 min, m/z 362); (16) 2-octenal (t_R:12.0 min, m/z 374); (17) octanal (t_R:12.2 min, m/z 376); (18) 2,4-NDE (t_R:12.2 min, m/z 386); (19) 2-nonenal (t_R:12.4 min, m/z 388); (20) nonanal (t_R:12.6 min, m/z 390); (21) 2,4-DDE (t_R:12.5 min, m/z 400); (22) ONE (t_R:11.5 min, m/z 402); (23) HNE (t_R:10.8 min, m/z 404); (24) decanal (t_R:13.0 min, m/z 404); (25) EDE (t_R:11.3 min, m/z 416); (26) 2-undecenal (t_R:13.1 min, m/z 416); (27) undecanal (t_R:13.3 min, m/z 418); (28) dodecanal (t_R:13.6 min, m/z 432); (29) tridecanal (t_R:13.9 min, m/z 446); (30) tetradecanal (t_R:14.3 min, m/z 460); (31) pentadecanal (t_R:14.6 min, m/z 474); (32) hexadecanal (t_R:14.8 min, m/z 488); (33) heptadecanal (t_R:15.1 min, m/z 502); (34) octadecanal (t_R:15.4 min, m/z 516); (35) secosterol-A (t_R:14.4 min, m/z 666); (36) secosterol-B (t_R:14.8 min, m/z 666); (IS) p-BOBA (t_R:11.8 min, m/z 460).

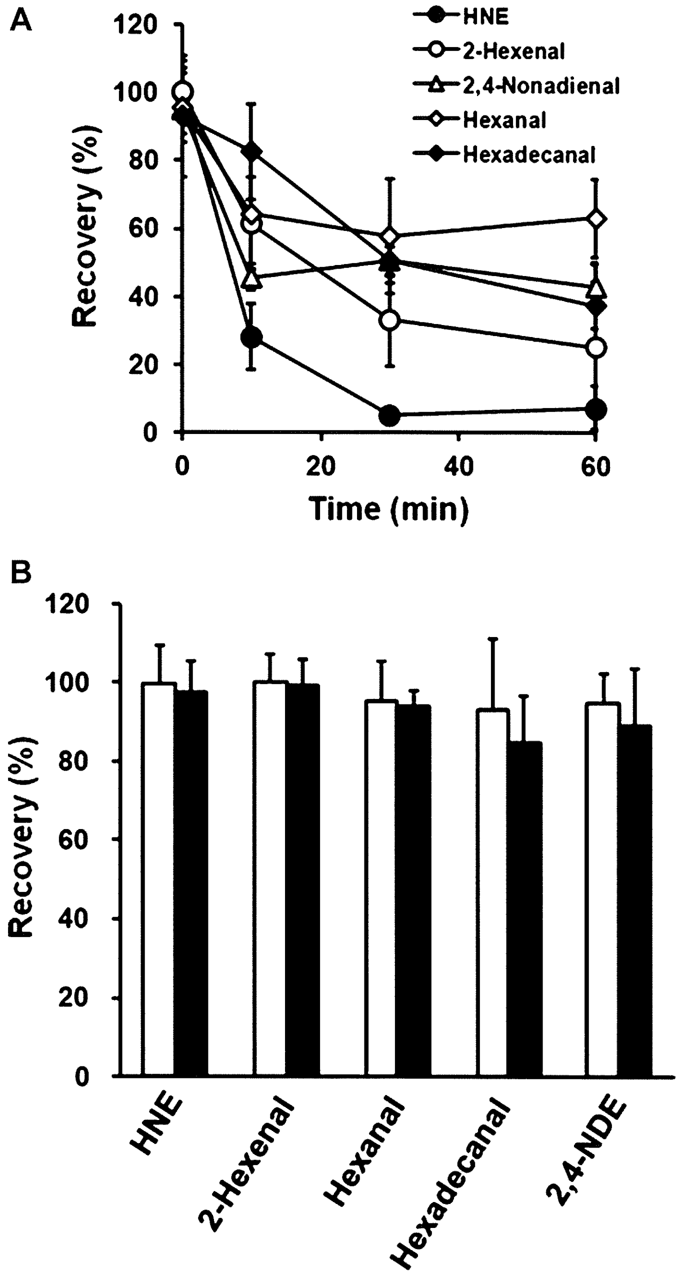

Fig. 3. Stabilities of the RCs in mice plasma. The plasma samples (100 μL) were spiked with five representative RCs, such as 4-hydroxy-2-alkenal (HNE), 2-alkenal (2-hexenal), and 2,4-alkadienal (2,4-NDE), as well as a short chain alkanal (hexanal) (5 pmol each) and a long chain alkanal (hexadecanal) (100 pmol). The spiked samples were stored on ice for 0–60 min (A) or stored at −80 °C for 4 weeks (B). The open and closed bars represent the recoveries of the RCs, which were determined immediately before and after being stored at −80 °C for 4 weeks.

analytical platform for studying the roles of RCs in the development and progression of oxidative stress related-disorders.

3.3. Comprehensive analyses of the lipophilic RCs present in mouse plasma samples

Our newly developed method was used to analyze the RC profiles of plasma samples obtained from C57BL/6J mice (10 weeks of age). Fig. 4 shows SRM chromatograms typical of those obtained for the free RCs detected in the mouse plasma samples. Fig. 5A shows the corresponding RCs maps, where all of the free RCs detected in the mouse plasma samples were plotted as circles as a function of their retention times (horizontal axis) and m/z values (vertical axis). The areas of the circles represent the intensities of peaks for the detected RCs relative to that of IS.

Four hundred and five peaks were detected in the plasma samples obtained from the normal C57BL/6J mice (based on an average of five determinations) following the elimination of the redundant peaks from the spectra, including the spike noise and artifactual DH derivatives (e.g., some of the solvents used in the current study were found to be contaminated with RCs). The RCs detected in the mouse plasma samples using this method were considered to be free RCs or those liberated from unstable Schiff base adducts.

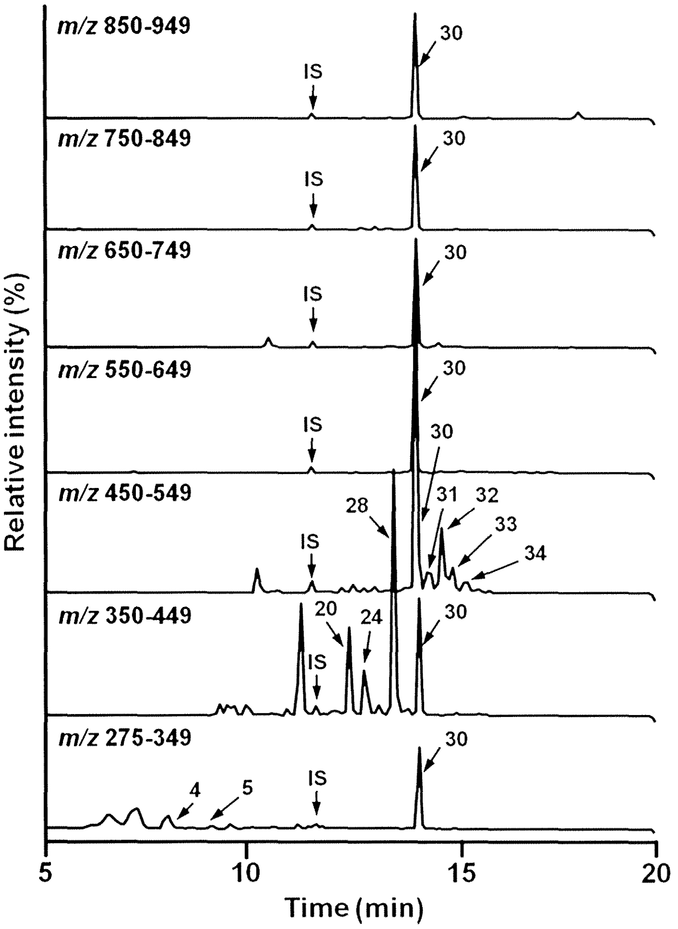

Fig. 4. Representative SRM chromatograms of the RC-DH derivatives, which were detected in the plasma samples obtained from normal C57BL/6J mice.

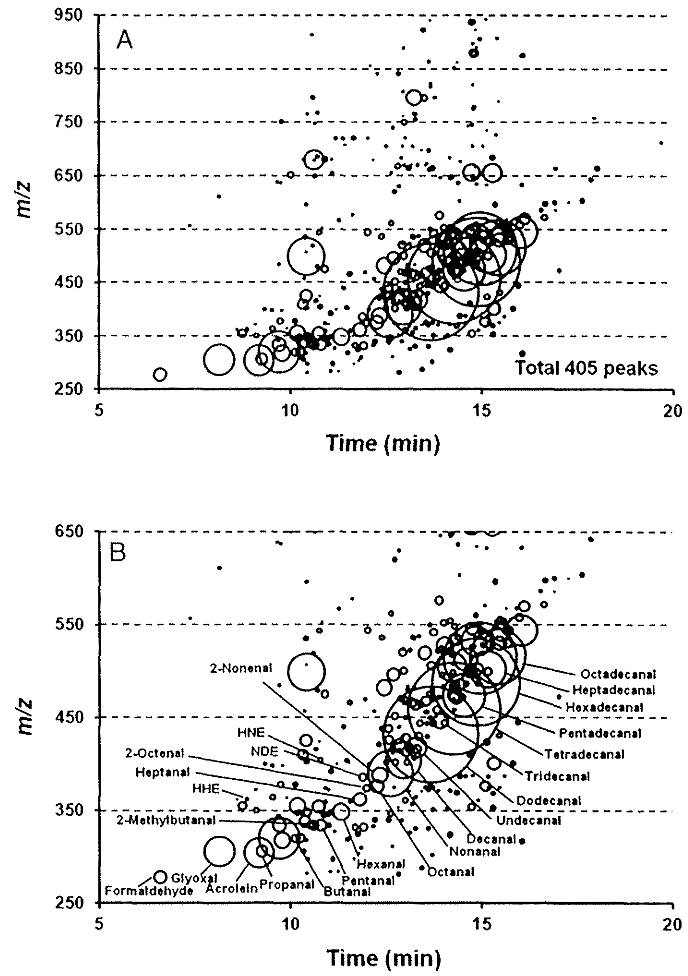

Fig. 5. RC maps of the plasma samples obtained from normal C57BL/6J mice (A). An enlarged view showing the names of some of the RCs identified through a comparison of their data with those of the authentic standards in Fig. 5A (B). In the RC map, the different RCs detected are shown as circles as a function of their LC retention times (horizontal axis) and *m/z* values (vertical axis). The area of each circle represents the relative intensity of the RC to that of IS.

Fig. 5B is an enlarged view of Fig. 5A, showing *m/z* values in the range of 250–650, together with the names of some of the RCs identified through a comparison of their data with those of the authentic RCs. A series of low molecular weight aldehydes, including formaldehyde (t_R: 6.8 min, *m/z* 278), acetaldehyde (t_R: 7.5 min, *m/z* 292), acrolein (t_R: 9.3 min, *m/z* 304), glyoxal (t_R: 8.4 min, *m/z* 306) and propanal (t_R: 9.3 min, *m/z* 306) are shown in the bottom left corner in Fig. 5B. Several large circles also appeared side by side on the diagonal in the center of the figure. As the retention times increased, the molecular weights of these peaks increased in *m/z* increments of 14. Based on a comparison of these peaks with those of the authentic RCs, it was established that they corresponded to several fatty aldehydes, including hexanal ($C_6H_{12}O$, t_R: 11.3 min, *m/z* 348), nonanal ($C_9H_{18}O$, t_R: 12.6 min, *m/z* 390) and hexadecanal ($C_{16}H_{32}O$, t_R: 14.8 min, *m/z* 488). Dodecanal ($C_{12}H_{24}O$) was determined to be the most abundant peak in the chromatogram with a retention time of 13.6 min and an *m/z* value of 432. Low concentrations of HHE (t_R: 8.9 min, *m/z* 362), NDE (t_R: 12.1 min, *m/z* 386), DDE (t_R: 12.5 min, *m/z* 400), ONE (t_R: 11.5 min, *m/z* 402), HNE (t_R: 10.8 min, *m/z* 404) and EDE (t_R: 11.3 min, *m/z* 416) were also detected. These RCs are known oxidation products, which are derived from PUFAs, such as linoleic acid (LA), arachidonic acid (AA) and docosahexaenoic acid (DHA). Acrolein can be derived from the oxidation of either DHA or AA, whereas hexanal and HNE can be derived from the oxidation of AA and LA. HHE is the major product of the oxidation of DHA and other ω-3 PUFAs [21–28].

A variety of fatty aldehydes between C1 (formaldehyde) and C18 (octadecanal) were detected in the plasma samples obtained from normal C57BL/6J mice (Fig. 5), with some of these fatty aldehydes being detected in large concentrations. Fatty aldehydes have been reported to undergo further biotransformations to afford fatty acids and alcohols [4,26,28–31]. Hexadecanal has been reported to form as one of the major products of the sphigosine-1-phosphate lyase-mediated degradation of dihydrosphingosine-1-phosphate (DHS1P) [32].

The peak with a retention time of 10.5 min and an *m/z* value of 334 was attributed to 2-methylbutanal, which has been reported to be formed by the oxidation of the aliphatic amino acid L-isoleucine with a myeloperoxidase-H_2O_2-chloride system [33].

Our newly developed method can be used to detect a large number of different free lipophilic RCs (regardless of their structure) including alkanals (e.g., hexanal and hexadecanal), 2-alkenals (e.g., 2-nonenal) and 4-hydroxy-2-alkenals (e.g., HNE and ONE), as well as structurally unknown RCs.

During the course of the current study, Siegel et al. [34] reported a similar method for the quantification and identification of various RCs in biological samples. Siegel's method involved the derivatization of RCs with *p*-toluensulfonylhydrazine and the subsequent detection of the derivatives by ultrahigh-performance liquid chromatography with ESI-MS. We believe that our newly developed method is comparable with that of Siegel et al. [34] in term of its specificity, sensitivity and repeatability properties for the analysis of a wide variety of RCs.

4. Conclusion

We have developed a novel analytical method for profiling the wide variety of different lipophilic RCs present in biological samples using LC/ESI-MS/MS with SRM. The method was found to be sensitive, reproducible, accurate and specific for RCs, and the analytical results obtained in the current were expressed as RC maps, which allowed for the types and levels of the different lipophilic RCs to be readily visualized. The results revealed that a large number of unidentified RCs were present in the mice plasma samples, and further studies are therefore needed to identify the structures of these compounds. This newly developed approach could be very useful for establishing the RC profiles of biological and environmental samples, as well as for studying the roles of lipid peroxidation in oxidative stress related-disorders and discovering new biomarkers for the early diagnosis of these diseases.

Acknowledgments

This work was supported in part by grants from the Japan Society for the Promotion of Science (JSPS) KAKENHI (grant nos. 24700838, 24680075 and 24300257 for ST, NM, and HO, respectively). This study was also supported by grants from the National Cancer Center Research and Development Fund 23-A-4 and 26-A-8) and Grants-in-Aids [Risk of Chemical Substance 2524301 (H25-Kagaku-ippan-004)] from the Ministry of Health, Labor and Welfare, Japan.

References

[1] M. Masoodi, A.A. Mir, N.A. Petasis, C.N. Serhan, A. Nicolaou, Simultaneous lipidomic analysis of three families of bioactive lipid mediators leukotrienes, resolvins, protectins and related hydroxy-fatty acids by liquid chromatography/electrospray ionisation tandem mass spectrometry, Rapid Commun. Mass Spectrom. 22 (2008) 75–83.
[2] E. Niki, Lipid peroxidation: physiological levels and dual biological effects, Free Radic. Biol. Med. 47 (2009) 469–484.
[3] F. Gueraud, M. Atalay, N. Bresgen, A. Cipak, P.E. Eckl, L. Huc, I. Jouanin, W. Siems, K. Uchida, Chemistry and biochemistry of lipid peroxidation products, Free Radic. Res. 44 (2010) 1098–1124.
[4] P.J. O'Brien, A.G. Siraki, N. Shangari, Aldehyde sources, metabolism, molecular toxicity mechanisms, and possible effects on human health, Crit. Rev. Toxicol. 35 (2005) 609–662.
[5] P.A. Grimsrud, H. Xie, T.J. Griffin, D.A. Bernlohr, Oxidative stress and covalent modification of protein with bioactive aldehydes, J. Biol. Chem. 283 (2008) 21837–21841.
[6] S. Bacot, N. Bernoud-Hubac, N. Baddas, B. Chantegrel, C. Deshayes, A. Doutheau, M. Lagarde, M. Guichardant, Covalent binding of hydroxy-alkenals 4-HDDE, 4-HHE, and 4-HNE to ethanolamine phospholipid subclasses, J. Lipid Res. 44 (2003) 917–926.
[7] S. Bacot, N. Bernoud-Hubac, B. Chantegrel, C. Deshayes, A. Doutheau, G. Ponsin, M. Lagarde, M. Guichardant, Evidence for in situ ethanolamine phospholipid adducts with hydroxyl-alkenals, J. Lipid Res. 48 (2007) 816–825.
[8] R.G. Salomon, X. Gu, Critical insights into cardiovascular disease from basic research on the oxidation of phospholipids: the γ-hydroxyalkenal phospholipid hypothesis, Chem. Res. Toxicol. 24 (2011) 1791–1802.
[9] W. Völkel, R. Alvarez-Sánchez, I. Weick, A. Mally, W. Dekant, A. Pähler, Glutathione conjugates of 4-hydroxy-2(E)-nonenal as biomarkers of hepatic oxidative stress-induced lipid peroxidation in rats, Free Radic. Biol. Med. 38 (2005) 1526–1536.
[10] W. Jian, S.H. Lee, C. Mesaros, T. Oe, M.V. Elipe, I.A. Blair, A novel 4-oxo-2(E)-nonenal-derived endogeneous thiadiazabicylo glutathione adduct formed during cellular oxidative stress, Chem. Res. Toxicol. 20 (2007) 1008–1018.
[11] K. Uchida, Role of reactive aldehyde in cardiovascular diseases, Free Radic. Biol. Med. 28 (2000) 1685–1696.
[12] U. Nair, H. Bartsch, J. Nair, Lipid peroxidation-induced DNA damage in cancer-prone inflammatory diseases: a review of published adduct types and levels in humans, Free Radic. Biol. Med. 43 (2007) 1109–1120.
[13] X.P. Luo, M. Yazdanpanah, N. Bhooi, D.C. Lehotay, Determination of aldehydes and other lipid peroxidation products in biological samples by gas chromatography–mass spectrometry, Anal. Biochem. 228 (1995) 294–298.
[14] G.A. Cordis, D.K. Das, W. Riedel, High-performance liquid chromatographic peak identification of 2,4-dinitrophenylhydrazine derivatives of lipid peroxidation aldehydes by photodiode array detection, J. Chromatogr. A 798 (1998) 117–123.
[15] C. Zwiener, T. Glauner, F.H. Frimmel, Method optimization for the determination of carbonyl compounds in disinfected water by DNPH derivatization and LC/ESI-MS-MS, Anal. Bioanal. Chem. 372 (2002) 615–621.
[16] S. Tomono, N. Miyoshi, K. Sato, Y. Ohba, H. Ohshima, Formation of cholesterol ozonolysis products through an ozone-free mechanism mediated by the myeloperoxidase-H_2O_2-chloride system, Biochem. Biophys. Res. Commun. 383 (2009) 222–227.
[17] S. Tomono, N. Miyoshi, H. Shiokawa, T. Iwabuchi, Y. Aratani, T. Higashi, H. Nukaya, H. Ohshima, Formation of cholesterol ozonolysis products in vitro and in vivo through a myeloperoxidase-dependent pathway, J. Lipid Res. 52 (2011) 87–97.
[18] N. Miyoshi, N. Iwasaki, S. Tomono, T. Higashi, H. Ohshima, Occurrence of cytotoxic 9-oxononanoyl secosterol aldehydes in human low-density lipoprotein, Free Radic. Biol. Med. 60 (2013) 73–79.
[19] D.K. Dalvie, J.P. O'Donnell, Characterization of polar urinary metabolites by ion-spray tandem mass spectrometry following dansylation, Rapid Commun. Mass Spectrom. 12 (1998) 419–422.
[20] P. Wentworth Jr., J. Nieva, C. Takeuchi, R. Galve, A.D. Wentworth, R.B. Dilley, G.A. DeLaria, A. Saven, B.M. Babior, K.D. Janda, A. Eschenmoser, R.A. Lerner, Evidence for ozone formation in human atherosclerotic arteries, Science 302 (2003) 1053–1056.
[21] T. Kaneko, S. Honda, S. Nakano, M. Matsuo, Lethal effects of a linoleic acid hydroperoxide and its autooxidation products, unsaturated aliphatic aldehydes, on human diploid fibroblasts, Chem. Biol. Interact. 63 (1987) 127–137.
[22] T. Kaneko, K. Kaji, M. Matsuo, Cytotoxicities of a linoleic acid hydroperoxide and its related aliphatic aldehydes toward cultured human umbilical vein endothelial cells, Chem. Biol. Interact. 67 (1988) 295–304.
[23] J.K. Beckman, M.J. Howard, H.L. Greene, Identification of hydroxyalkenals formed from omega-3 fatty acids, Biochem. Biophys. Res. Commun. 169 (1990) 75–80.
[24] F.J. Van Kuijk, L.L. Holte, E.A. Dratz, 4-Hydroxyhexenal: a lipid peroxidation product derived from oxidized docosahexaenoic acid, Biochim. Biophys. Acta 1043 (1990) 116–118.
[25] S.H. Lee, T. Oe, I.A. Blair, Vitamin C-induced decomposition of lipid hydroperoxides to endogenous genotoxins, Science 292 (2001) 2083–2086.
[26] P. Spiteller, W. Kern, J. Reiner, G. Spiteller, Aldehydic lipid peroxidation products derived from linoleic acid, Biochem. Biophys. Acta 1531 (2001) 188–208.
[27] K. Warner, W.E. Neff, W.C. Byrdwell, H.W. Gardner, Effect of oleic and linoleic acid on the production of deep-fried odor in heated triolein and trilinolein, J. Agric. Food Chem. 49 (2001) 899–905.
[28] Y. Kawai, S. Takeda, J. Terao, Lipidomic analysis for lipid peroxidation-derived aldehydes using gas chromatography-mass spectrometry, Chem. Res. Toxicol. 20 (2007) 99–107.
[29] H. Esterbauer, G. Jurgens, O. Quehenberger, E. Koller, Autoxidation of human low density lipoprotein: loss of polyunsaturated fatty acid and vitamin E and generation of aldehydes, J. Lipid Res. (1987) 495–509.
[30] S. Stadelmann-Ingrand, S. Favreliere, B. Fauconneau, G. Mauco, C. Tallineau, Plasmalogen degratdation by oxidative stress: production and disappearance of specific fatty aldehydes and fatty alpha-hydroxyaldehydes, Free Radic Biol. Med. 31 (2001) 1263–1271.
[31] K. Watschinger, E.R. Werner, Alkylglycerol monooxygenase, IUBMB Life 65 (2013) 366–372.
[32] E.V. Berdyshev, J. Goya, I. Gorshkova, G.D. Prestwich, H.S. Byun, R. Bittman, V. Natarajan, Characterization of sphingosine-1-phosphate lyase activity by electrospray ionization-liquid chromatography/tandem mass spectrometry quantitation of (2E)-hexadecenal, Anal. Biochem. 408 (2011) 12–18.
[33] S.L. Hazen, F.F. Hsu, A. d'Avignon, J.W. Heinecke, Human neutrophils employ myeloperoxidase to convert alpha-amino acids to a battery of reactive aldehydes: a pathway for aldehyde generation at sites of inflammation, Biochemistry 37 (1998) 6864–6873.
[34] D. Siegel, A.C. Meinema, H. Permentier, G. Hopfgartner, R. Bischoff, Integrated quantification and identification of aldehydes and ketones in biological samples, Anal. Chem. 86 (2014) 5089–5100.

Biochemical and Biophysical Research Communications 446 (2014) 702–708

Contents lists available at ScienceDirect

Biochemical and Biophysical Research Communications

journal homepage: www.elsevier.com/locate/ybbrc

Review

Implications of cholesterol autoxidation products in the pathogenesis of inflammatory diseases

Noriyuki Miyoshi [a,*], Luigi Iuliano [b,*], Susumu Tomono [a], Hiroshi Ohshima [a]

[a] Laboratory of Biochemistry, Graduate School of Integrated Pharmaceutical and Nutritional Sciences, Graduate Program in Food and Nutritional Sciences, University of Shizuoka, Shizuoka 422-8526, Japan

[b] Department of Medico-Surgical Sciences and Biotechnologies, Laboratory of Vascular Biology and Mass Spectrometry, Sapienza University of Rome, Latina 04100, Italy

ARTICLE INFO

Article history:
Available online 9 January 2014

Keywords:
Cholesterol autoxidation
Inflammation
Oxidative stress
Oxysterols
Secosterol

ABSTRACT

There is rising interest in non-enzymatic cholesterol oxidation because the resulting oxysterols have biological activity and can be used as non-invasive markers of oxidative stress *in vivo*. The preferential site of oxidation of cholesterol by highly reactive species is at C_7 having a relatively weak carbon–hydrogen bond. Cholesterol autoxidation is known to proceed via two distinct pathways, a free radical pathway driven by a chain reaction mechanism (type I autoxidation) and a non-free radical pathway (type II autoxidation). Oxysterols arising from type II autoxidation of cholesterol have no enzymatic correlates, and singlet oxygen ($^1\Delta gO_2$) and ozone (O_3) are the non-radical molecules involved in the mechanism. Four primary derivatives are possible in the reaction of cholesterol with singlet oxygen via ene addition and the formation of 5α-, 5β-, 6α- and 6β-hydroxycholesterol preceded by their respective hydroperoxyde intermediates. The reaction of ozone with cholesterol is very fast and gives rise to a complex array of oxysterols. The site of the initial ozone reaction is at the $\Delta_{5,6}$ –double bond and yields 1,2,3-trioxolane, a compound that rapidly decomposes into a series of unstable intermediates and end products. The downstream product 3β-hydroxy-5-oxo-5,6-secocholestan-6-al (sec-A, also called 5,6-secosterol), resulting from cleavage of the B ring, and its aldolization product (sec-B) have been proposed as a specific marker of ozone-associated tissue damage and ozone production *in vivo*. The relevance of specific ozone-modified cholesterol products is, however, hampered by the fact sec-A and sec-B can also arise from singlet oxygen via Hock cleavage of 5α-hydroperoxycholesterol or via a dioxietane intermediate. Whatever the mechanism may be, sec-A and sec-B have no enzymatic route of production *in vivo* and are reportedly bioactive, rendering them attractive biomarkers to elucidate oxidative stress-associated pathophysiological pathways and to develop pharmacological agents.

© 2014 Elsevier Inc. All rights reserved.

Contents

Abbreviations: Aβ, amyloid-β; Chol-OOHs, cholesterol hydroperoxides; C27 3β -HSD, 3β-hydroxy-Δ^5-C_{27}-steroid oxidoreductase; DNPH, dinitrophenyl hydrazine; DH, dansyl hydrazine; GP, Girard P; GC/MS, gas chromatography/mass spectrometry; HMP, 2-hydrazino-1-methylpyridine; LC/MS, liquid chromatography/mass spectrometry; LOD, limit of detection; LOO˙, lipid peroxyl radicals; LO˙, lipid alkoxyl radicals; MBP, myelin basic protein; MPO, myeloperoxidase; PBH, pyrenebutyric hydrazine; PHGPx, phospholipid-hydroperoxide glutathione peroxidase; sec-A, 3β-hydroxy-5-oxo-5,6-secocholestan-6-al; secA-COOH, 3β-hydroxy-5-oxo-secocholestan-6-oic acid; sec-B, 3β-hydroxy-5β-hydroxy-B-norcholestane-6β-carboxaldehyde; secB-COOH, 3β-hydroxy-5β-hydroxy-B-norcholestane-6-oic acid; 5α-Chol-OOH, 5α-cholesterol-hydroperoxide; 5β-Chol-OOH, 5β-cholesterol-hydroperoxide; 6α-Chol-OOH, 6α-cholesterol-hydroperoxide; 6β-Chol-OOH, 6β-cholesterol-hydroperoxide; 7α-OHC, 7α-hydroxycholesterol; 7α-Chol-OOH, 7α-cholesterol-hydroperoxide; 7β-Chol-OOH, 7β-cholesterol-hydroperoxide; 24-OHC, 24-hydroxycholesterol; 27-OHC, 27-hydroxycholesterol.

* Corresponding authors. Fax: +81 54 264 5530 (N. Miyoshi). Fax: +39 06 62 29 1089 (L. Iuliano).
E-mail addresses: miyoshin@u-shizuoka-ken.ac.jp (N. Miyoshi), luigi.iuliano@uniroma1.it (L. Iuliano).

0006-291X/$ - see front matter © 2014 Elsevier Inc. All rights reserved.
http://dx.doi.org/10.1016/j.bbrc.2013.12.107

1. Introduction

Oxysterols are derivatives of cholesterol containing one or more oxygen atoms, other than the OH group on C_3, as hydroxyl, keto, epoxide or peroxyde group – that is mounted on the A and B ring or on the side chain. Oxysterols can be generated either enzymatically, mainly by the group of cytochrome (CYP) P450 family, or by autoxidation [1]. In brief, in biological systems oxygenation on side-chain is almost exclusively enzymatic, while that on the A and B ring can occur both enzymatically and by autoxidation.

Oxysterols arising from enzymatic synthesis can be used as markers of their respective cytochrome activity. Circulating 7α-hydroxycholesterol (7α-OHC), a starting intermediate in the biosynthesis of bile acids [2], correlates with the activity of CYP7A1 [3], 7α-hydroxy-4-cholesten-3-one, a conversion product of 7α-OHC is formed by the microsomal 3β-hydroxy-Δ^5-C_{27}-steroid oxidoreductase (C27 3β-HSD) [4], 4β-hydroxycholesterol can be used as an endogenous marker of CYP3A4 and CYP3A5 activity [5], 24S-hydroxycholesterol (24-OHC) is the product of the brain-specific cholesterol 24-hydroxylase (CYP46A1) [6,7], 27-hydroxycholesterol (27-OHC) is formed by the mitochondrial enzyme sterol 27-hydroxylase (CYP27A1), which is widely distributed in tissues [8,9]. Examples of oxysterols forming enzymes different than the cyt450 family are cholesterol 25-hydroxylase [10] and oxidosqualene cyclase [11], which produce 25-hydroxycholesterol and 24(S),25-epoxycholesterol, respectively, and cholesterol epoxide hydrolase that converts 5,6-epoxydes into cholesterol-triol [12].

The susceptibility of cholesterol to non-enzymatic oxidation has generated considerable interest in oxysterols as potential markers for the non-invasive study of oxidative stress *in vivo*. Additional interest in oxysterols stems from the biological activity of many oxysterols that is useful to elucidate pathophysiological pathways in human diseases and for pharmacological purposes [13]. Cholesterol autoxidation proceeds via two distinct pathways, a free radical pathway driven by a chain reaction mechanism (type I) and a non-free radical pathway (type II), which is driven stoichiometrically by highly reactive oxygen species [13,14]. The unique cholesterol double bond between carbons 5 and 6 is the most vulnerable site for oxidation by free radicals and highly reactive species [15].

2. Cholesterol autoxidation

Type I autoxidation involves initiation and propagation reactions. Free radicals provide the initiation step by hydrogen abstraction, formation of a carbon centered radical and subsequent oxygen capture. Afterwards, the process advances through free radical intermediates – including, peroxyl radicals (LOO°) and alkoxyl radicals (LO°) – that in turn recruit additional non-oxidized molecules and provoke the spreading of the process via a chain-reaction, the propagation phase.

Despite the hydrogen bond-dissociation energy of C_7-cholesterol is higher than the hemolytic cleavage of allylic hydrogens in polyunsaturated fatty acids [16], entropic factors determine a predominant role of cholesterol oxidation in cellular membranes [17].

A multitude of oxysterols can be formed upon type I autoxidation, but analytical issues restrain the number of species usable as markers of oxidative stress in biological matrices. The species that actually perform well on GC/MS, which is the gold standard for oxysterols measurement, are: 4α- and 7β-hydoxycholesterol, 5α,6α- and 5β,6β-epoxides, and 7-ketocholesterol [13]. Recent studies from Porter and co-workers have established the product distribution of several oxysterols obtained through the free radical chain oxidation of the cholesterol precursor 7-dehydrocholesterol [18].

In type II autoxidation the main molecules that are involved in cholesterol oxidation are the non-radical species singlet oxygen and ozone. Singlet oxygen is formed by an input of energy, such as photoactivation, the Russell mechanism, based on the decomposition of lipid hydroperoxides, and by the reactions of hypochlorous acid and hydrogen peroxide. The following primary species are possible in the reaction of cholesterol with singlet oxygen via ene addition: 5α-cholesterol-hydroperoxide (5α-Chol-OOH), 5β-cholesterol-hydroperoxide (5β-Chol-OOH), 6α-cholesterol-hydroperoxide (6α-Chol-OOH), 6β-cholesterol-hydroperoxide (6β-Chol-OOH), and Chol-1,2-dioxetane. The formation of 5α-Chol-OOH is highly favored at a rate of approximately one order of magnitude higher than that of 6α-Chol-OOH and 6β-Chol-OOH [19]. Minor products of ozone-driven cholesterol oxidation are 5α,6α- and 5β,6β-epoxides, which have been found to form in ethyl acetate [20], but their participation in a physiological environment is not reported. The 7α- and 7β-Chol-OOH are formed during the reaction of singlet oxygen with cholesterol and generated indirectly by the allylic rearrangement of 5α-Chol-OOH [21], which takes place at high peroxidation levels but is negligible under limited cholesterol oxidation (<5%) [22]. Cholesterol hydroperoxides are susceptible to 1 e^- reduction that gives rise to alkoxyl- and peroxyl-radical intermediates that, in turn, can trigger chain reactions and amplify the free radical cascade of cholesterol oxidation and the oxidative damage. All cholesterol hydroperoxides are expected to be equally susceptible to 1 e^- reduction in the presence of metal catalysts. Similar rate constants have been reported for the reduction of 5α-Chol-OOH and 6α-Chol-OOH formation during incubation with an iron-based redox cycling system in a homogeneous solution in which cholesterol was the only chain-carrying species [19]. The potency of 5α-Chol-OOH and 7α-Chol-OOH as chain initiators is comparable [23]. Cholesterol hydroperoxides (Chol-OOHs) are resistant to direct 2 e^- reduction that is catalyzed by Se-dependent glutathione peroxidase [24]. This means that Chol-OOHs have a potential long half-life in cells. The only enzyme capable of catalyzing the reduction of Chol-OOHs to stable diols, is the phospholipid-hydroperoxide glutathione peroxidase (PHGPx) [25]. However, the reduction of Chol-OOH by PHGPx is 6 times slower compared to the reduction of phospholipid hydroperoxides [26], and shows different rate constants ranging from 0.8×10^2 min^{-1} for 5α-Chol-OOH to $\approx 6 \times 10^2$ min^{-1} for 6α-Chol-OOH and 6β-Chol-OOH [19]. Thus, 5α-Chol-OOH results the most abundant product of singlet oxygen reaction with cholesterol, and the least resistant to detoxification via PHGPx. The forward products arising from type-II cholesterol autoxidation are cholesterol aldehydes.

3. Cholesterol aldehydes: ozone or not ozone?

3β-Hydroxy-5-oxo-5,6-secocholestan-6-al (sec-A), the major cholesterol ozonolysis products [20], is unstable in physiological aqueous conditions, such as culture medium containing serum, and is readily converted to its aldolization product 3β-hydroxy-5β-hydroxy-B-norcholestane-6β-carboxaldehyde (sec-B) (Fig. 1) [27]. In part, sec-A and sec-B are further converted to their oxidized forms 3β-hydroxy-5-oxo-secocholestan-6-oic acid (secA-COOH) and 3β-hydroxy-5β-hydroxy-B-norcholestane-6-oic acid (secB-COOH) in culture media and probably *in vivo* [27]. Recently, ozonolysis products of the major cholesteryl fatty acid esters transported in human LDL have been reported [28]. Under a flux of ozone, cholesteryl palmitate gives rise to palmitoyl-sec-A and palmitoyl-sec-B. Instead, ozonolysis of cholesterol esterified with unsaturated fatty acids oleate and linoleate admits the initial

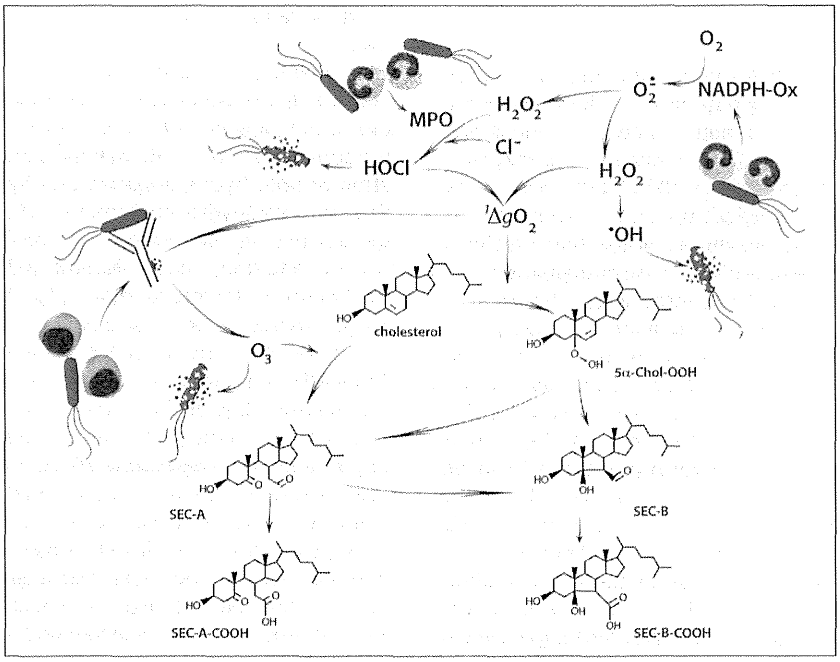

Fig. 1. Schematic representation of secosterols formation during the inflammatory response. Phagocytic cells recruited after a bacterial insult, are activated to produce highly reactive oxygen species through two enzymatic systems, i.e. NADPH-oxidase (NADPH-ox) and Myeloperoxidase (MPO) that contribute to bacterial killing. The formation of ozone by an antibody catalyzed reaction that uses singlet oxygen as substrate, has been proposed by Wentworth et al. [32,70,71] as an ancestral primary immune-response mechanism additional to the well-known superoxide-hydrogen peroxide-HOCl system. Ozone (O_3) and singlet oxygen ($^1\Delta gO_2$) may catalyze the formation of secosterols by promoting cholesterol autoxidation.

isolation of cholesteryl-9-oxononanoate and the subsequent appearance of both the fatty acid and cholesteryl moiety oxidation products, i.e. 9-oxononanoyl-sec-A and 9-oxononanoyl-sec-B [28]. These compounds derived from cholesterol/cholesterol esters ozonolysis exert potent biological activities including the denaturation of proteins and strong cytotoxicity in different cells lines (see below). High levels of sec-A and sec-B have been detected in human atherosclerotic plaques [29] and tissues samples of brains affected by neurodegeneration, such as Alzheimer's disease and Lewy body dementia [30,31], suggesting that increased formation of these compounds may be associated with inflammation-related diseases. Wentworth et al. [29] conducted pioneering works on secosterols and advised sec-A and sec-B as potential diagnostic markers of endogenous ozone production. They proposed a novel mechanisms for the unprecedented formation of ozone *in vivo* consisting of reactive oxygen species cascade (Fig. 1): (a) superoxide generation by activated neutrophil, (b) dismutation into hydrogen peroxide, (c) hypochlorous acid (HOCl) formation by myeloperoxidase (MPO), (d) singlet oxygen generation by the reaction of HOCl and hydrogen peroxide, and afterwards (e) formation of ozone from the singlet oxygen in an antibody-catalyzed water oxidation pathway [32,33]. A similar mechanism for the production of ozone-like reactive species from singlet oxygen in an amino acids-catalyzed water oxidation pathway was also reported [34]. However others have argued against the ozone-dependent mechanism of sec-A formation *in vivo* [35–37], and pointed out an alternative pathway for the formation of sec-A and sec-B. Uemi et al. [38] proposed a mechanism based on the Hock cleavage of 5α-Chol-OOH or a Chol-1,2-dioxetane intermediate formed by the reaction of cholesterol with singlet oxygen. Others provided evidence for sec-A and sec-B generation by the reaction of cholesterol with singlet oxygen produced by 1-methylnaphthalene-4-endoperoxide in phosphate buffer [39], and by the MPO–H_2O_2–Cl system [39]. Taken together these data point to a duplicate mechanism of sec-A and sec-B formation involving either ozone or singlet oxygen. Garner et al. [40] recently reported the development of a specific fluorogenic probes for ozone detections that, eventually, may help to investigate the role of ozone in pathophysiology. Being sec-B the predominant species formed during singlet oxygen-mediated cholesterol oxidation (sec-B is about 5–10 times higher than sec-A), the ratio sec-A to sec-B has been proposed as a surrogate measure to decipher the ozone-dependent and independent oxidation of cholesterol [39]. On the other hand, sec-A occurs as the dominant species formed by ozone in aqueous buffer system [41], and by phorbol-12-myristate-3-acetate-activated neutrophil in culture [27]. In addition, we were able to observe a time-dependent elevation of sec-A and sec-B in plasma after injecting lipopolysaccaride to C57BL/6j mice, but not in MPO-deficient mice. Besides, basal levels of sec-A and sec-B in the plasma of MPO-deficient mice were lower than the value found in wild type mice, but sec-A was barely detectable [27]. Sec-B was shown to be formed by aldolization of sec-A and, also, in an ozone-independent pathway via 5α-OOH-Chol or cholesterol-1,2-dioxetane [38]. Sec-B detected in the plasma of MPO-deficient mice, therefore, could be formed by the reaction of cholesterol with singlet oxygen generated *in vivo*, although its exact origin is currently unknown. Taken together these findings advise the occurrence of ozone-mediated reaction *in vivo* even if no conclusive evidences so far could be drawn for ozone production *in vivo*.

4. Biological activity of secosterols

The aldehydic function of secosterols is highly reactive and efficiently forms Schiff bases with ε- or N-terminal amino groups of proteins and with phosphatidylethanolamine, relevantly connected with atherosclerosis and a number of diseases associated with protein misfolding.

Wentworth et al. [29] reported that incubation of human LDL with either sec-A or sec-B led to time-dependent changes in the circular dichroism spectra of apoB-100, consistent with an altered secondary structure, and increased atherogenicity, e.g. the secosterol-modified LDL was avidly taken up by macrophage leading to foam cell formation. Sec-A was shown to randomly modify the 6 different Lys residues of ApoC-II, as well as apolipoprotein that in the absence of lipids has conformational instability and undergoes fibrillization [42]. Sec-A accelerated ApoC-II polymerization with concurrent increase in thioflavin fluorescence [42], a signature of amyloidogenesis [43]. Interestingly, secA-COOH, which lacks the aldehydic functionality and is unable to form Schiff bases, was also able to accelerate ApoC-II fibril formation, albeit at a lesser extent, suggesting that non-covalent mechanisms may support secosterol-dependent ApoC-II amyloidogenesis [42]. These findings are relevant to the mechanisms of atherosclerosis because amyloid deposits are present in 50–60% of atherosclerotic lesions [44] and ApoC-II is a prominent component of these deposits [45]. Concentrations of secosterols are reportedly elevated in the cortex of patients with Lewy body dementia [31], a disease associated with intra-neuronal accumulation of α-synuclein in the form of amyloid fibrils or Lewy bodies. Sec-A, sec-B, and secoA-COOH have been shown to accelerate α-synuclein aggregation *in vitro*, and more interestingly secA-COOH was even more potent in forwarding the process [31]. Amyloidogenicity of amyloid-β (Aβ) is considered a crucial player of Alzheimer disease but an open question is the 2–3 order of magnitude disparity between the critical concentration to induce aggregation, which is in the micromolar range, and the actual concentration of Aβ at tissue level, which is in the nanomolar range [46]. Secosterols have been shown to effectively reduce below 100 nM the critical concentration of Aβ to aggregate [30,47]. Among the Aβ adducts with secosterol, Lys-16 Aβ modification formed amorphous aggregates fast and at very low concentrations of Aβ (20 nM), followed by the Lys-28 and Asp-1. Besides, the aggregates resulting from Lys-secosterols adducts were more toxic to primary rat cortical neuron [48]. Sec-A and sec-B in brain samples of patients affected by neurodegenerative disease approach concentrations of up 1 μM [30,49] that are suitable to covalently modify Aβ and increase its amyloidogenicity [30,31,47,50,51]. Sec-A and sec-B have been reported to induce structural change to myelin basic protein (MBP) relevant to the context of demyelinating diseases [52]. MBP accounts for approximately 30% of the total myelin protein, and is responsible for adhesion and stabilization of the intracellular surfaces of myelin layers. By reacting with MBP, secosterols have been shown to increase the surface exposure of the immunodominant epitope, decrease the surface exposure of the cathepsin D binding, and reduce the size and structural stability of MBP-induced aggregates. As a consequence of these alterations in the structure and function, MBP is unable to maintain the integrity of the myelin sheath and becomes vulnerable to autoimmune attack. In line to that which is observed with secosterol-initiated misfolding of Aβ and α-synuclein, sec-A and sec-B have been reported to induce misfolding of wild-type p53 [53]. The tumor suppressor protein p53 functions to maintain the integrity of the genome, and its activation in response to DNA damage promotes cell-cycle arrest in G1 phase or apoptosis. Upon incubation with secosterols, p53 undergoes polymerization that anticipates the formation of amyloid fibrillary aggregates. This misfolding renders p53 unable to bind to DNA and to induce transactivation of p21 [53]. Given that inflammation is the fuel for secosterols formation and that inflammation functions in all stages of tumor development, secosterols provide a chemical link to understand cancer carrying inactive p53.

Light-chain deposition disease is a severe, often fatal, clinical condition in which amyloid or amorphous deposits, as a consequence of antibody light chain aggregation, accumulate in the heart and/or kidney. Sec-A and sec-B have been reported to accelerate aggregation of human antibody kappa and lambda light chains *in vitro* under physiologically relevant conditions, causing an amorphous-type aggregation that is thioflavin and Congo red negative for both the kappa and lambda light chains [54]. Given the inflammatory microenvironment of secosterol production and its association with antibodies, the secosterol-induced protein misfolding is consistent with a pathophysiological role in light-chain deposition disease.

While the above reported studies show secosterols as playing deleterious roles by promoting misfolding of varied proteins, sec-B has unexpectedly been shown to inhibit the misfolding of a truncated murine mutant prion protein. Incubation of sec-B with a murine prion protein, paradoxically, induced stabilization of the native form of the prion and inhibited the generation of the disease-causing scrapie form [55]. The inhibition was specific for sec-B, where structural analogues were ineffective, offering a promising tool to develop new pharmacological active compounds to treat prion disease.

Additionally, secosterols have been reported to affect membrane and enzyme function. It was shown that secosterols bound phosphatidylethanolamine and phosphatidylserine via Schiff base formation, and also reduced biophysical parameters of membrane stability, which could be associated with various pathogenic insults [56–58]. Recently Genaro-Mattos and co-workers [59] reported that sec-B covalently bound and anchored cytochrome c to mitochondrial mimetic membranes, although its physiological role is still under investigation. Sec-A, but not sec-B, reportedly inhibited endothelial- and neuronal-type of nitric oxide synthase (NOS) activities, probably mediated by adduct formations with lysine residues on these enzymes [60]. The biochemical and biophysical properties of secosterols could be associated with their noxious activity on cells. Several studies have found that sec-A and sec-B induce cell death in various cell lines, including human B-lymphocytes (WI-L2), T-lymphocytes (Jurkat), vascular smooth muscle cells (VSMC), abdominal aorta endothelial cells (HAEC), murine tissue macrophages (J774.1), and an alveolar macrophage cell line (MH-S) [29]. Sathishkumar et al. [61] reported that sec-A exerted about 2-fold higher cytotoxicity than 5,6β-epoxy-Chol in hypothalamic neuron GT1-7 cells. Several pathways have been postulated for secosterol-triggered cell death, including the caspase-3/7-dependent pathway and the mitochondrial and death receptor pathway in cardiomyocyte H9c2 cells [62,63], the reactive oxygen species-dependent pathway in hypothalamic neuron GT1-7 cells [61,64], a mitochondrial death pathway in macrophage J774 cells, and the mitogen-activated protein kinase pathway in hepatocarcinoma HepG2 and Huh7 cells [65]. Moreover, secA-COOH and secB-COOH showed strong cytotoxic activities in human acute promyelocytic leukemia HL-60 cells [66]. Recently, it has been reported that 9-oxononanoyl-secA and 9-oxononanoyl-secB – ozonolysis products of cholesteryl-oleate and cholesteryl-linoleate present in human LDL – exert potent cytotoxicity towards HL-60 cells [28]. Their activity is stronger than other cytotoxic oxysterols, exhibiting EC50s of 10–20 μM, which were very similar against various cell lines tested.

5. *In vivo* detection

An overview of methods, biological samples investigated and levels of secosterols reported to date in the literature is shown in Table 1. For the analysis of sec-A and sec-B in biological or clinical samples, HPLC separation with UV, fluorescence, or MS detection have been widely employed. In general, lipid extracts of blood or tissue samples containing sec-A and sec-B are derivatized with hydrazine derivatives, such as dinitrophenylhydrazine (DNPH) [29,67,72]. To perform higher sensitivity detection, derivatization with dansyl hydrazine (DH, LOD = 1 fmol in [27,31,39]), 1-pyrenebutyric hydrazine (PBH; LOD = 10 fmol in [68]), Girard P (GP) hydra-

Table 1
Detections of sec-A and sec-B in biological samples.

Tissues/fluids	Species	Forms	Equipments	Concentrations	N	Ref
Lung	Rat (SD) exposed to ozone	Sec-A-DNPH	HPLC-UV	ND		72
		Sec-B-DNPH		ND		
Atherosclerotic plaque	Human	Sec-A-DNPH	HPLC-UV and LC-MS	6.8 - 61.3 pmol/mg	n=11	29
Plasma	Human (atherosclerotic patients)	Sec-B-DNPH		70 - 1690 nM	n=8	
Brain	Human (Alzheimer patients)	Sec-A-DNPH + Sec-B-DNPH	HPLC-UV and LC-MS	0.44 pmol/mg	n=4	30
	Human (Control)	Sec-A-DNPH + Sec-B-DNPH		0.35 pmol/mg	n=7	
Brain	Human (Lewy body dementia)	Sec-A-DNSL + Sec-B-DNSL	HPLC-F	0.21 uM	n=15	31
	Age-matched control	Sec-A-DNSL + Sec-B-DNSL		0.09 uM	n=18	
Brain	Rat	Sec-A-GP	LC-MS	~100 pg/mg		49
		Sec-B-GP		~300 pg/mg		
	Human	Sec-A-GP + Sec-B-GP		150 pg/mg		
Plasma	Mouse (C57BL/6)	Sec-A-DNSL	LC-MS/MS with IS (^{13}C-sec-A + ^{13}C-sec-B)	0.5 ± 0.2 nM	n=8	27
		Sec-B-DNSL		1.1 ± 0.3 nM	n=8	
	Mouse (C57BL/6 MPO-KO)	Sec-A-DNSL		0.03 ± 0.1 nM	n=7	
		Sec-B-DNSL		0.5 ± 0.4 nM	n=7	
Liver	Mouse (C57BL/6)	Sec-B-DNSL		126.0 ± 42.7 pmol/g	n=8	
	Mouse (C57BL/6 MPO-KO)	Sec-B-DNSL		62.2 ± 21.6 pmol/g	n=7	
Plasma	Human (healthy volunteers)	Sec-A-HMP	LC-MS/MS with IS (^{13}C-sec-A + ^{13}C-sec-B)	23.6 ± 16.6 nM	n=10	69
		Sec-B-HMP		27.3 ± 41.0 nM	n=10	
	Mouse (C57BL/6)	Sec-A-HMP		1.4 ± 0.7 pmol/g	n=3	
		Sec-B-HMP		4.3 ± 0.8 pmol/g	n=3	
Brain		Sec-A-HMP		10.4 ± 16.3 pmol/g	n=3	
		Sec-B-HMP		110.9 ± 10.6 pmol/g	n=3	
Liver		Sec-A-HMP		34.1 ± 21.6 pmol/g	n=3	
		Sec-B-HMP		161.5 ± 56.3 pmol/g	n=3	
Lung		Sec-A-HMP		29.1 ± 1.3 pmol/g	n=3	
		Sec-B-HMP		80.4 ± 1.4 pmol/g	n=3	

zine (LOD = 2.7 fmol in [49]), or 2-hydrazino-1-methylpyridine (HMP; LOD = 10–50 amol in [69]). Using these derivatizing reagents, sec-A and sec-B present in blood or tissues were detectable as secosterol–hydrazone derivatives by HPLC-fluorescence detector and LC–MS (Table 1). Griffiths and co-workers reported levels of sec-A and sec-B in rat brain of ~100 pg/mg (240 pmol/g) and ~300 pg/mg (720 pmol/g), respectively, determined after derivatization with GP hydrazine [49]. Sec-A and sec-B in human brain were also analyzed by HPLC-UV or LC–MS after derivatization with DNPH resulting in levels of (sec-A + sec-B) 0.44 pmol/mg in Alzheimer's patients ($n = 4$) and 0.35 pmol/mg in control subjects ($n = 7$) [30]. In addition, increased levels of secosterols (sec-A + sec-B) were observed in the cortex of brain affected by Lewy body dementia (0.213 μM, $n = 15$) compared to those of age-matched controls (0.093 μM, $n = 18$) in analysis done by HPLC-fluorescence detector and LC–MS after DH derivatization [31]. Wentworth and co-worker analyzed DNPH-derivatives of sec-A and sec-B in organic extracts of human atherosclerotic plaque by LC–MS, and found them in the ranges of 6.8–61.3 pmol/mg plaque [29]. Elevated levels of sec-B were also observed in the plasma of these patients (70–1690 nM) compared to those of controls subjects [29]. We have recently developed a highly sensitive isotope dilution method to detect sec-A and sec-B as HMP derivatives by LC–ESI–MS/MS, and using 3,4-^{13}C-sec-A and 3,4-^{13}C-sec-B as internal standards [69]. We found levels of sec-A and sec-B of 23.6 ± 16.6 nM and 27.3 ± 41.0 nM, respectively, in human plasma ($n = 10$). The levels of sec-A and sec-B were respectively 1.4 ± 0.7 and 4.3 ± 0.8 nM in the plasma, 10.4 ± 16.3 and 110.9 ± 10.6 pmol/g in the brain, 34.1 ± 21.6 and 161.5 ± 56.3 pmol/g in the liver and 29.1 ± 1.3, and 80.4 ± 1.4 pmol/g in the lung of C57BL/6j mice ($n = 3$). In addition, ozonolysis products of cholesteryl-oleate and cholesteryl-linoleate, 9-oxononanoyl-sec-A and 9-oxononanoyl-sec-B, were found in human LDL at levels of 16.5 ± 5.4 and 11.3 ± 3.9 pmol/mg LDL protein, respectively [28]. Notably, the values of cholesterol aldehydes in biological samples differ widely among the different laboratories. As sec-A is very unstable, at least the use of stable-isotope labeled internal standards in secosterol analysis is mandatory.

Although formation mechanisms of secosterols are not still fully unveiled, elevated levels of secosterols have been observed in various tissues collected from different inflammatory diseases. Sec-A, sec-B, and other related compounds including secA-COOH, secB-COOH, and 9-oxononanoyl secosterols exert strong biological activities compared to other oxysterols. Further studies are warranted to elucidate the mechanisms of secosterols formation *in vivo* and their pathological roles in relation to pathogenesis of several inflammatory diseases.

Acknowledgments

This work was supported in part by JSPS KAKENHI Grants (24680075 to NM, 24700838 to ST, and 24300257 to HO).

References

[1] I.A. Pikuleva, Cholesterol-metabolizing cytochromes P450: implications for cholesterol lowering, Expert Opin. Drug Metab. Toxicol. 4 (2008) 1403–1414.
[2] I. Bjorkhem, G. Eggertsen, Genes involved in initial steps of bile acid synthesis, Curr. Opin. Lipidol. 12 (2001) 97–103.
[3] I. Bjorkhem, E. Reihner, B. Angelin, S. Ewerth, J.E. Akerlund, K. Einarsson, On the possible use of the serum level of 7alpha-hydroxycholesterol as a marker for increased activity of the cholesterol 7alpha-hydroxylase in humans, J. Lipid Res. 28 (1987) 889–894.
[4] A. Lovgren-Sandblom, M. Heverin, H. Larsson, E. Lundstrom, J. Wahren, U. Diczfalusy, I. Bjorkhem, Novel LC–MS/MS method for assay of 7alpha-hydroxy-4-cholesten-3-one in human plasma. Evidence for a significant extrahepatic metabolism, J. Chromatogr. B: Anal. Technol. Biomed. Life Sci. 856 (2007) 15–19.
[5] U. Diczfalusy, J. Miura, H.K. Roh, R.A. Mirghani, J. Sayi, H. Larsson, K.G. Bodin, A. Allqvist, M. Jande, J.W. Kim, E. Aklillu, L.L. Gustafsson, L. Bertilsson, 4Beta-hydroxycholesterol is a new endogenous CYP3A marker: relationship to CYP3A5 genotype, quinine 3-hydroxylation and sex in Koreans, Swedes and Tanzanians, Pharmacogenet. Genomics 18 (2008) 201–208.
[6] D. Lutjohann, O. Breuer, G. Ahlborg, I. Nennesmo, A. Siden, U. Diczfalusy, I. Bjorkhem, Cholesterol homeostasis in human brain: evidence for an age-dependent flux of 24S-hydroxycholesterol from the brain into the circulation, Proc. Natl. Acad. Sci. U S A 93 (1996) 9799–9804.

[7] Y. Ohyama, S. Meaney, M. Heverin, L. Ekstrom, A. Brafman, M. Shafir, U. Andersson, M. Olin, G. Eggertsen, U. Diczfalusy, E. Feinstein, I. Bjorkhem, Studies on the transcriptional regulation of cholesterol 24-hydroxylase (CYP46A1): marked insensitivity toward different regulatory axes, J. Biol. Chem. 281 (2006) 3810–3820.

[8] N.B. Javitt, 25R,26-Hydroxycholesterol revisited: synthesis, metabolism, and biologic roles, J. Lipid Res. 43 (2002) 665–670.

[9] N.B. Javitt, Oxysteroids: a new class of steroids with autocrine and paracrine functions, Trends Endocrinol. Metab. 15 (2004) 393–397.

[10] E.G. Lund, T.A. Kerr, J. Sakai, W.P. Li, D.W. Russell, CDNA cloning of mouse and human cholesterol 25-hydroxylases, polytopic membrane proteins that synthesize a potent oxysterol regulator of lipid metabolism, J. Biol. Chem. 273 (1998) 34316–34327.

[11] J. Wong, C.M. Quinn, A.J. Brown, Synthesis of the oxysterol, 24(S), 25-epoxycholesterol, parallels cholesterol production and may protect against cellular accumulation of newly-synthesized cholesterol, Lipids Health Dis. 6 (2007) 10.

[12] G. Segala, Medina P. de, L. Iuliano, C. Zerbinati, M.R. Paillasse, E. Noguer, F. Dalenc, B. Payre, V.C. Jordan, M. Record, S. Silvente-Poirot, M. Poirot, 5,6-Epoxy-cholesterols contribute to the anticancer pharmacology of tamoxifen in breast cancer cells, Biochem. Pharmacol. 86 (2013) 175–189.

[13] L. Iuliano, Pathways of cholesterol oxidation via non-enzymatic mechanisms, Chem. Phys. Lipids 164 (2011) 457–468.

[14] A.W. Girotti, Lipid hydroperoxide generation, turnover, and effector action in biological systems, J. Lipid Res. 39 (1998) 1529–1542.

[15] O. Wintersteiner, S. Bergström, The products formed by the action of oxygen on colloidal solutions of cholesterol, J. Biol. Chem. 137 (1941) 785–786.

[16] H.W. Gardner, Oxygen radical chemistry of polyunsaturated fatty acids, Free Radical Biol. Med. 7 (1989) 65–86.

[17] D. Neshchadin, F. Palumbo, M.S. Sinicropi, I. Andreu, G. Gescheidta, M.A. Miranda, Topological control in radical reactions of cholesterol in model dyads, Chem. Sci. 4 (2013) 1608–1614.

[18] L. Xu, Z. Korade, N.A. Porter, Oxysterols from free radical chain oxidation of 7-dehydrocholesterol: product and mechanistic studies, J. Am. Chem. Soc. 132 (2010) 2222–2232.

[19] W. Korytowski, M. Wrona, A.W. Girotti, Radiolabeled cholesterol as a reporter for assessing one-electron turnover of lipid hydroperoxides, Anal. Biochem. 270 (1999) 123–132.

[20] J. Gumulka, L.L. Smith, Ozonization of cholesterol, J. Am. Chem. Soc. 105 (1983) 1972–1979.

[21] L.J. Athelstan, J. Beckwith, A.G. Davies, I.G.E. Davison, A. Maccoll, M.H. Mruzek, The mechanism of the rearrangement of allylic hydroperoxides 5α-hydroperoxy-3-β-hydroxycholest-6ene- and 7α-hydroperoxy-3-beta-hydroxycholest-5-ene, J. Chem. Soc., Perkin Trans. 22 (1989) 815–824.

[22] W. Korytowski, G.J. Bachowski, A.W. Girotti, Photoperoxidation of cholesterol in homogeneous solution, isolated membranes, and cells: comparison of the 5 alpha- and 6 beta-hydroperoxides as indicators of singlet oxygen intermediacy, Photochem. Photobiol. 56 (1992) 1–8.

[23] W. Korytowski, P.G. Geiger, A.W. Girotti, Lipid hydroperoxide analysis by high-performance liquid chromatography with mercury cathode electrochemical detection, Methods Enzymol. 300 (1999) 23–33.

[24] J.P. Thomas, A.W. Girotti, Photooxidation of cell membranes in the presence of hematoporphyrin derivative: reactivity of phospholipid and cholesterol hydroperoxides with glutathione peroxidase, Biochim. Biophys. Acta 962 (1988) 297–307.

[25] J.P. Thomas, M. Maiorino, F. Ursini, A.W. Girotti, Protective action of phospholipid hydroperoxide glutathione peroxidase against membrane-damaging lipid peroxidation. In situ reduction of phospholipid and cholesterol hydroperoxides, J. Biol. Chem. 265 (1990) 454–461.

[26] J.P. Thomas, P.G. Geiger, M. Maiorino, F. Ursini, A.W. Girotti, Enzymatic reduction of phospholipid and cholesterol hydroperoxides in artificial bilayers and lipoproteins, Biochim. Biophys. Acta 1045 (1990) 252–260.

[27] S. Tomono, N. Miyoshi, H. Shiokawa, T. Iwabuchi, Y. Aratani, T. Higashi, H. Nukaya, H. Ohshima, Formation of cholesterol ozonolysis products in vitro and in vivo through a myeloperoxidase-dependent pathway, J. Lipid Res. 52 (2011) 87–97.

[28] N. Miyoshi, N. Iwasaki, S. Tomono, T. Higashi, H. Ohshima, Occurrence of cytotoxic 9-oxononanoyl secosterol aldehydes in human low-density lipoprotein, Free Radical Biol. Med. 60 (2013) 73–79.

[29] P. Wentworth Jr., J. Nieva, C. Takeuchi, R. Galve, A.D. Wentworth, R.B. Dilley, G.A. DeLaria, A. Saven, B.M. Babior, K.D. Janda, A. Eschenmoser, R.A. Lerner, Evidence for ozone formation in human atherosclerotic arteries, Science 302 (2003) 1053–1056.

[30] Q. Zhang, E.T. Powers, J. Nieva, M.E. Huff, M.A. Dendle, J. Bieschke, C.G. Glabe, A. Eschenmoser, P. Wentworth Jr., R.A. Lerner, J.W. Kelly, Metabolite-initiated protein misfolding may trigger Alzheimer's disease, Proc. Natl. Acad. Sci. U S A 101 (2004) 4752–4757.

[31] D.A. Bosco, D.M. Fowler, Q. Zhang, J. Nieva, E.T. Powers, P. Wentworth Jr., R.A. Lerner, J.W. Kelly, Elevated levels of oxidized cholesterol metabolites in Lewy body disease brains accelerate alpha-synuclein fibrilization, Nat. Chem. Biol. 2 (2006) 249–253.

[32] P. Wentworth Jr., J.E. McDunn, A.D. Wentworth, C. Takeuchi, J. Nieva, T. Jones, C. Bautista, J.M. Ruedi, A. Gutierrez, K.D. Janda, B.M. Babior, A. Eschenmoser, R.A. Lerner, Evidence for antibody-catalyzed ozone formation in bacterial killing and inflammation, Science 298 (2002) 2195–2199.

[33] B.M. Babior, C. Takeuchi, J. Ruedi, A. Gutierrez, P. Wentworth Jr., Investigating antibody-catalyzed ozone generation by human neutrophils, Proc. Natl. Acad. Sci. U S A 100 (2003) 3031–3034.

[34] K. Yamashita, T. Miyoshi, T. Arai, N. Endo, H. Itoh, K. Makino, K. Mizugishi, T. Uchiyama, M. Sasada, Ozone production by amino acids contributes to killing of bacteria, Proc. Natl. Acad. Sci. U S A 105 (2008) 16912–16917.

[35] H. Sies, Ozone in arteriosclerotic plaques: searching for the "smoking gun", Angew. Chem., Int. Ed. Engl. 43 (2004) 3514–3515.

[36] L.L. Smith, Oxygen, oxysterols, ouabain, and ozone: a cautionary tale, Free Radical Biol. Med. 37 (2004) 318–324.

[37] W.A. Pryor, K.N. Houk, C.S. Foote, J.M. Fukuto, L.J. Ignarro, G.L. Squadrito, K.J. Davies, Free radical biology and medicine: it's a gas, man!, Am J. Physiol. Regul. Integr. Comp. Physiol. 291 (2006) R491–R511.

[38] M. Uemi, G.E. Ronsein, S. Miyamoto, M.H. Medeiros, Mascio P. Di, Generation of cholesterol carboxyaldehyde by the reaction of singlet molecular oxygen [O_2 ($^1\Delta_g$)] as well as ozone with cholesterol, Chem. Res. Toxicol. 22 (2009) 875–884.

[39] S. Tomono, N. Miyoshi, K. Sato, Y. Ohba, H. Ohshima, Formation of cholesterol ozonolysis products through an ozone-free mechanism mediated by the myeloperoxidase–H_2O_2–chloride system, Biochem. Biophys. Res. Commun. 383 (2009) 222–227.

[40] A.L. Garner, C.M. St Croix, B.R. Pitt, G.D. Leikauf, S. Ando, K. Koide, Specific fluorogenic probes for ozone in biological and atmospheric samples, Nat. Chem. 1 (2009) 316–321.

[41] A.D. Wentworth, B.D. Song, J. Nieva, A. Shafton, S. Tripurenani, P. Wentworth Jr., The ratio of cholesterol 5,6-secosterols formed from ozone and singlet oxygen offers insight into the oxidation of cholesterol in vivo, Chem. Commun. (Cambridge, U.K.) 21 (2009) 3098–3100.

[42] C.R. Stewart, L.M. Wilson, Q. Zhang, C.L. Pham, L.J. Waddington, M.K. Staples, D. Stapleton, J.W. Kelly, G.J. Howlett, Oxidized cholesterol metabolites found in human atherosclerotic lesions promote apolipoprotein C-II amyloid fibril formation, Biochemistry 46 (2007) 5552–5561.

[43] D.M. Hatters, C.E. MacPhee, L.J. Lawrence, W.H. Sawyer, G.J. Howlett, Human apolipoprotein C-II forms twisted amyloid ribbons and closed loops, Biochemistry 39 (2000) 8276–8283.

[44] C. Rocken, J. Tautenhahn, F. Buhling, D. Sachwitz, S. Vockler, A. Goette, T. Burger, Prevalence and pathology of amyloid in atherosclerotic arteries, Arterioscler. Thromb. Vasc. Biol. 26 (2006) 676–677.

[45] L.A. Medeiros, T. Khan, J.B. El Khoury, C.L. Pham, D.M. Hatters, G.J. Howlett, R. Lopez, K.D. O'Brien, K.J. Moore, Fibrillar amyloid protein present in atheroma activates CD36 signal transduction, J. Biol. Chem. 279 (2004) 10643–10648.

[46] P.D. Mehta, T. Pirttila, B.A. Patrick, M. Barshatzky, S.P. Mehta, Amyloid beta protein 1–40 and 1–42 levels in matched cerebrospinal fluid and plasma from patients with Alzheimer disease, Neurosci. Lett. 304 (2001) 102–106.

[47] J. Bieschke, Q. Zhang, E.T. Powers, R.A. Lerner, J.W. Kelly, Oxidative metabolites accelerate Alzheimer's amyloidogenesis by a two-step mechanism, eliminating the requirement for nucleation, Biochemistry 44 (2005) 4977–4983.

[48] K. Usui, J.D. Hulleman, J.F. Paulsson, S.J. Siegel, E.T. Powers, J.W. Kelly, Site-specific modification of Alzheimer's peptides by cholesterol oxidation products enhances aggregation energetics and neurotoxicity, Proc. Natl. Acad. Sci. U S A 106 (2009) 18563–18568.

[49] K. Karu, M. Hornshaw, G. Woffendin, K. Bodin, M. Hamberg, G. Alvelius, J. Sjovall, J. Turton, Y. Wang, W.J. Griffiths, Liquid chromatography-mass spectrometry utilizing multi-stage fragmentation for the identification of oxysterols, J. Lipid Res. 48 (2007) 976–987.

[50] H. Komatsu, L. Liu, I.V. Murray, P.H. Axelsen, A mechanistic link between oxidative stress and membrane mediated amyloidogenesis revealed by infrared spectroscopy, Biochim. Biophys. Acta 1768 (2007) 1913–1922.

[51] I.V. Murray, L. Liu, H. Komatsu, K. Uryu, G. Xiao, J.A. Lawson, P.H. Axelsen, Membrane-mediated amyloidogenesis and the promotion of oxidative lipid damage by amyloid beta proteins, J. Biol. Chem. 282 (2007) 9335–9345.

[52] N.K. Cygan, J.C. Scheinost, T.D. Butters, P. Wentworth Jr., Adduction of cholesterol 5,6-secosterol aldehyde to membrane-bound myelin basic protein exposes an immunodominant epitope, Biochemistry 50 (2011) 2092–2100.

[53] J. Nieva, B.D. Song, J.K. Rogel, D. Kujawara, L. Altobel 3rd, A. Izharrudin, G.E. Boldt, R.K. Grover, A.D. Wentworth, P. Wentworth Jr., Cholesterol secosterol aldehydes induce amyloidogenesis and dysfunction of wild-type tumor protein p53, Chem. Biol. 18 (2011) 920–927.

[54] J. Nieva, A. Shafton, L.J. Altobell 3rd, S. Tripuraneni, J.K. Rogel, A.D. Wentworth, R.A. Lerner, P. Wentworth Jr., Lipid-derived aldehydes accelerate light chain amyloid and amorphous aggregation, Biochemistry 47 (2008) 7695–7705.

[55] J.C. Scheinost, D.P. Witter, G.E. Boldt, J. Offer, P. Wentworth Jr., Cholesterol secosterol adduction inhibits the misfolding of a mutant prion protein fragment that induces neurodegeneration, Angew. Chem., Int. Ed. Engl. 48 (2009) 9469–9472.

[56] E. Wachtel, D. Bach, R.F. Epand, A. Tishbee, R.M. Epand, A product of ozonolysis of cholesterol alters the biophysical properties of phosphatidylethanolamine membranes, Biochemistry 45 (2006) 1345–1351.

[57] D. Bach, E. Wachtel, I.R. Miller, Kinetics of Schiff base formation between the cholesterol ozonolysis product 3-beta-hydroxy-5-oxo-5,6-secocholestan-6-al and phosphatidylethanolamine, Chem. Phys. Lipids 157 (2009) 51–55.

[58] D. Bach, R.F. Epand, R.M. Epand, I.R. Miller, E. Wachtel, The oxysterol 3beta-hydroxy-5-oxo-5,6-secocholestan-6-al changes the phase behavior and

structure of phosphatidylethanolamine–phosphatidylcholine mixtures, Chem. Phys. Lipids 164 (2011) 672–679.

[59] T.C. Genaro-Mattos, P.P. Appolinario, K.C. Mugnol, C. Bloch Jr., I.L. Nantes, Mascio.P. Di, S. Miyamoto, Covalent binding and anchoring of cytochrome c to mitochondrial mimetic membranes promoted by cholesterol carboxyaldehyde, Chem. Res. Toxicol. 26 (2013) 1536–1544.

[60] Y.L. Lai, S. Tomono, N. Miyoshi, H. Ohshima, Inhibition of endothelial- and neuronal-type, but not inducible-type, nitric oxide synthase by the oxidized cholesterol metabolite secosterol aldehyde: implications for vascular and neurodegenerative diseases, J. Clin. Biochem. Nutr. 50 (2012) 84–89.

[61] K. Sathishkumar, S.N. Murthy, R.M. Uppu, Cytotoxic effects of oxysterols produced during ozonolysis of cholesterol in murine GT1-7 hypothalamic neurons, Free Radical Res. 41 (2007) 82–88.

[62] K. Sathishkumar, M. Haque, T.E. Perumal, J. Francis, R.M. Uppu, A major ozonation product of cholesterol, 3β-hydroxy-5-oxo-5,6-secocholestan-6-al, induces apoptosis in H9c2 cardiomyoblasts, FEBS Lett. 579 (2005) 6444–6450.

[63] K. Sathishkumar, X. Gao, A.C. Raghavamenon, N. Parinandi, W.A. Pryor, R.M. Uppu, Cholesterol secoaldehyde induces apoptosis in H9c2 cardiomyoblasts through reactive oxygen species involving mitochondrial and death receptor pathways, Free Radical Biol. Med. 47 (2009) 548–558.

[64] K. Sathishkumar, X. Xi, R. Martin, R.M. Uppu, Cholesterol secoaldehyde, an ozonation product of cholesterol, induces amyloid aggregation and apoptosis in murine GT1-7 hypothalamic neurons, J. Alzheimers Dis. 11 (2007) 261–274.

[65] S. Anticoli, M. Arciello, A. Mancinetti, Martinis.M. De, L. Ginaldi, L. Iuliano, C. Balsano, 7-Ketocholesterol and 5,6-secosterol modulate differently the stress-activated mitogen-activated protein kinases (MAPKs) in liver cells, J. Cell Physiol. 222 (2010) 586–595.

[66] S. Tomono, Y. Yasue, N. Miyoshi, H. Ohshima, Cytotoxic effects of secosterols and their derivatives on several cultured cells, Biosci. Biotechnol. Biochem. 77 (2013) 651–653.

[67] K. Wang, E. Bermudez, W.A. Pryor, The ozonation of cholesterol: separation and identification of 2,4-dinitrophenylhydrazine derivatization products of 3 beta-hydroxy-5-oxo-5,6-secocholestan-6-al, Steroids 58 (1993) 225–229.

[68] F.V. Mansano, R.M. Kazaoka, G.E. Ronsein, F.M. Prado, T.C. Genaro-Mattos, M. Uemi, Mascio.P. Di, S. Miyamoto, Highly sensitive fluorescent method for the detection of cholesterol aldehydes formed by ozone and singlet molecular oxygen, Anal. Chem. 82 (2010) 6775–6781.

[69] S. Tomono, N. Miyoshi, M. Ito, T. Higashi, H. Ohshima, A highly sensitive LC–ESI-MS/MS method for the quantification of cholesterol ozonolysis products secosterol-A and secosterol-B after derivatization with 2-hydrazino-1-methylpyridine, J. Chromatogr., B: Anal. Technol. Biomed. Life Sci. 879 (2011) 2802–2808.

[70] D. Datta, N. Vaidehi, X. Xu, W.A. Goddard 3rd, Mechanism for antibody catalysis of the oxidation of water by singlet dioxygen, Proc. Natl. Acad. Sci. U S A 99 (2002) 2636–2641.

[71] A.D. Wentworth, L.H. Jones, P. Wentworth Jr., K.D. Janda, R.A. Lerner, Antibodies have the intrinsic capacity to destroy antigens, Proc. Natl. Acad. Sci. U S A 97 (2000) 10930–10935.

[72] W.A. Pryor, K. Wang, E. Bermudez, Cholesterol ozonation products as biomarkers for ozone exposure in rats, Biochem. Biophys. Res. Commun. 188 (1992) 618–623.

The Journal of Toxicological Sciences (J. Toxicol. Sci.)
Vol.39, No.3, 499-505, 2014

Original Article

MWCNT causes extensive damage to the ciliated epithelium of the trachea of rodents

Teruya Ohba[1], Jiegou Xu[2], David B. Alexander[2], Akane Yamada[1], Jun Kanno[3], Akihiko Hirose[4], Hiroyuki Tsuda[2] and Yuji Imaizumi[1]

[1]*Department of Molecular and Cellular Pharmacology, Nagoya City University Graduate School of Pharmaceutical Sciences, 3-1 Tanabedori, Mizuhoku, Nagoya 467-8603, Japan*
[2]*Laboratory of Nanotoxicology, Nagoya City University, 3-1 Tanabedori, Mizuhoku, Nagoya 467-8603, Japan*
[3]*Division of Cellular and Molecular Toxicology, 1-18-1 Kamiyoga, Setagaya-ku, Tokyo 158-8501, Japan*
[4]*Division of Risk Assessment, National Institute of Health Sciences, 1-18-1 Kamiyoga, Setagaya-ku, Tokyo 158-8501, Japan*

(Received February 19, 2014; Accepted April 8, 2014)

ABSTRACT — The ciliated tracheobronchial epithelium plays an important role in the excretion of inhaled dust. While many reports indicate that inhaled multi-walled carbon nanotubes (MWCNT) induce inflammation and proliferative changes in the lung and pleura, their effects on the upper airway have not been reported. Two different types of MWCNTs, MWCNT-L (8 μm in length and 150 nm in diameter) and MWCNT-S (3 μm in length and 15 nm in diameter), were examined for their effect on the trachea as well as the bronchus and lung. *In vitro*, the movement of the cilia of primary tracheal epithelial cells was impaired by treatment with the 2 MWCNTs. Rats were treated with 0.3 ml of a 250 μg/ml suspension of MWCNTs on days 1, 4, and 7, and sacrificed on day 8. Extensive loss of ciliated cells and replacement by flat cells without cilia was observed in the trachea. Deposition of MWCNTs and occasional squamous cell metaplasia were found in the regenerative granulation tissue. The proportion of the lesion to the transverse section of the trachea was vehicle, 0; MWCNT-L, 27.2 ± 10.5; MWCNT-S, 32.1 ± 15.8 (both MWCNTs, $p < 0.001$ vs vehicle). The amount of cilia showed significant decrease in the MWCNT-L treated rats ($p < 0.05$). In contrast to the trachea lesions, the number of inflammatory foci in the lung was greater in the MWCNT-S than in the MWCNT-L treated rats. Our results indicate that both MWCNTs caused extensive damage to the ciliated epithelium of the trachea. This damage may prolong the deposition of inhaled MWNCT in the lung.

Key words: MWCNT, Tracheal damage, Ciliated epithelium, Rat

INTRODUCTION

Multi-walled carbon nanotubes (MWCNT) are a newly developed material with potential applications in many fields including the biomedical field. The high aspect ratio of MWCNT is similar to that of asbestos and has led to concern that exposure to MWCNT might cause asbestos-like lung diseases (Bonner, 2010; Donaldson *et al.*, 2010; Nagai and Toyokuni, 2010). Many reports have indicated that exposure of rats to MWCNT induces inflammation, fibrosis and oxidative stress in the lung and pleura (Mercer *et al.*, 2010, 2013; Xu *et al.*, 2012). To date, *in vivo* studies have focused on the toxicity of MWCNT in the lung and pleura, and nothing has been reported regarding the effect of MWCNT on the epithelium of the trachea.

The tracheal and primary branch of the bronchial epithelium is mainly composed of ciliated cells and some goblet cells. The ciliated cells are responsible for carrying out inhaled dust particles in the throat by their ciliary transportation movement. Thus, the ciliated cells play a pivotal role in the defense of the airway against inhaled particle matter. Several environmental factors such as cigarette smoke (Simet *et al.*, 2010) and diesel gas particles (Li *et al.*, 2011) have been shown to impair ciliated cell functions, resulting in increased pulmonary deposition. Zinc oxide nanoparticles have been reported to induce proliferation of airway epithelial cells and goblet cell hyperplasia (Cho *et al.*, 2011) and transient epithelial hyperplasia of the terminal bronchiole (Xu *et al.*,

Correspondence: Yuji Imaizumi (E-mail: yimaizum@phar.nagoya-cu.ac.jp)

2014). Although several reports indicate that MWCNT have some toxic effects on bronchial epithelial cells *in vitro* (Hirano *et al.*, 2010; Lindberg *et al.*, 2009; Rotoli *et al.*, 2008), the effect on the upper airway in animals remains unknown. In the present study, we investigated the effects of MWCNT on the tracheal epithelium *in vitro* and *in vivo* and the bronchus and lung *in vivo* after short-term exposure.

MATERIALS AND METHODS

Animals

8-12 week old C57BL/6N male mice (Japan SLC Inc., Shizuoka, Japan) and 6-7 week old Wistar/ST rats were obtained from Japan SLC Inc. Rats were housed in the Animal Center of Nagoya City University Graduate School of Pharmaceutical Sciences and maintained on a 12 hr light/12 hr dark cycle and received Oriental MF basal diet (Oriental Yeast Co. Ltd., Tokyo, Japan) and water *ad libitum*. The study was conducted according to the Guidelines for the Care and Use of Laboratory Animals of Nagoya City University Graduate School of Pharmaceutical Sciences, and the experimental protocol was approved by the Nagoya City University Animal Care and Use Committee (H24-p-12).

Preparation of MWCNT and Fluorescent Microspheres (FMS)

We used two types of MWCNTs, MWCNT-L and MWCNT-S, which are grown in the vapor phase. According to the manufacturer's information, the primary size of MWCNT-L is 150 nm in mean diameter and 8 μm in mean length, and the primary size of MWCNT-S is 15 nm in mean diameter and 3 μm in mean length. Five milligrams of MWCNT-L or MWCNT-S were suspended in 20 ml of saline containing 0.5% Pluronic F68 (PF68, non-ionic, biocompatible amphiphillic block copolymers, Sigma-Aldrich, St Louis, MO, USA) and homogenized for 1 min at 3,000 rpm in a Polytron PT1600E bench-top homogenizer (Kinematika AG, Littau, Switzerland) 4 times. The suspensions were sonicated for 30 min shortly before use to minimize aggregation. The concentration of the MWCNTs was 250 μg/ml. Both MWCNT-L and MWCNT-S dispersed well in the vehicle solution. MWCNT-L showed single fibers with a needle-like shape under scanning electron microscope (SEM) observation, but gradually formed agglomerates over time. Since MWCNT-S are tangled fibers, it showed cotton-like aggregation in suspension under SEM observation. However, they did not form larger agglomerates: incubation in suspension up to 7 days (data not shown). Fluorescent Microspheres (FMS) were purchased from Invitrogen (TetraSpeckTM microspheres, 500 nm in diameter) and suspended by sonication at 250 μg/ml in saline containing 0.5% PF68.

Isolation of single ciliated cells

Isolation of single ciliated cells was as previously reported (Ma *et al.*, 2006). Briefly, the tracheal epithelium was separated from the cartilage and cut into pieces of approximately 0.1 × 0.1 cm. The tissue was incubated in phosphate-buffered saline containing NaCl 137 mM, KCl 2.7 mM, $CaCl_2$ 0.9 mM, $MgCl_2$ 0.5 mM, Na_2HPO_4 8 mM, KH_2PO_4 1.47 mM and d-glucose 5 mM, pH 7.4 (PBS-g) supplemented with 13 U/ml papain (Sigma), 1 mg/ml bovine serum albumin (Sigma-Aldrich) and 1 mg/ml 1,4-dithiothreitol (Wako Chemicals Co. Ltd., Osaka, Japan). Cells were then dispersed several times with a fire-polished Pasteur pipette and re-suspended in PBS-g and used immediately.

In vitro study

The isolated mouse tracheal epithelial cells were maintained in high glucose Dulbecco's modified Eagle's medium (DMEM, Sigma) supplemented with 10% fetal bovine serum (FBS), 1 U/ml penicillin G, and 0.1 mg/ml streptomycin sulfate, at 37°C, 5% CO_2. The cells were then exposed for 10 min to vehicle, FMS, MWCNT-L, or MWCNT-S in FMS or MWCNT suspensions to a final concentration of 10 μg/ml. Media was then replaced by fresh media. The cells were observed 10 min and 12 and 18 hr after addition of fresh media and the proportion of cells with ciliary movement per total ciliated cells was determined. For each group, approximately 500 cells per dish in three separate dishes were counted.

Rat study

Male Wistar rats aged 6-7 weeks were treated with 0.3 ml of 250 μg/ml MWCNT-L or MWCNT-S (3 rats each) suspended in PF68 vehicle on days 1, 4, and 7. The suspension was administered by a microsprayer (series IA-1B Intratracheal Aerosolizer; Penn-century, Philadelphia, PA, USA) with the tip of the microsprayer just inside the entrance of the trachea (Xu *et al.*, 2012). Administration was done in synchronization with spontaneous inhalation. The rats were sacrificed 24 hr after the last dosing (day 8) under deep anesthesia with isoflurane. The trachea, bronchus and lung were excised and fixed in 4% paraformaldehyde solution. The trachea was transversely cut into 3 pieces, upper, middle and lower parts, and the tracheal sections and the bronchus and lungs were routinely processed for paraffin embedding, sectioning and histological examination.

Histology and Immunostaining

Haematoxylin-Eosin (H&E) stained slides of the trachea; bronchus and lung were examined by board pathologists. The epithelial lesions in each tracheal section were measured with the image analyzing function (Nikon, Tokyo, Japan) and expressed as the ratio of the length of the lesion to the whole length of the tracheal section. The number of granulation foci of the lung sections were counted and expressed as number/cm^2 lung tissue. Localization of MWCNT fibers in the trachea and lung tissue were determined with polarized light microscopy (Olympus BX51N-31P-O, Tokyo, Japan) at × 400 and × 1,000 magnification. Immunostaining of acetyled tublin, a specific marker for cilia, was performed using mouse polyclonal anti-acetyled tublin antibody (Sigma Aldrich). The antibody was diluted 1:1,000 in PBS containing 5% goat albumin and applied to deparaffinized and blocked slides, and the slides were incubated at 4°C overnight. The next day, the slides were washed 3 times in PBS and then incubated for 2 hr with Alexa 488-conjugated goat anti-mouse IgG (Molecular Probe, Eugene, OR, USA) diluted 1:1,000. After washing 3 times in PBS, the slides were counterstained with DAPI (Vector laboratories, Burlingame, CA, USA). Immunostained sections were observed using an A1R laser scanning confocal microscope (Nikon). The ratio of the fluorescent intensity of acetyled tublin in the top layer of cells of the tracheal ciliated epithelium to the fluorescent intensity of DAPI in the underlying submucosal tissue was measured. This ratio was used to compare the intensity of acetyled tublin fluorescence in the different samples. Fluorescence intensity was determined with NIS Elements software (version 3.10; Nikon).

Statistical Analysis

Statistical significance was examined using Tukey's test. *P* values less than 0.05 were considered to be statistically significant.

RESULTS

In vitro study

Cultures of ciliated cells were incubated in growth media with vehicle (PF68), fluorescent microspheres (FMS), or MWCNT for 10 min. During the 10 min incubation in media containing FMS, FMS in contact with the cilia and/or cell surface could readily be located (white arrow in Fig. 1A in bottom panel), however, 10 min after replacing the FMS containing media with standard growth media, cell-associated FMS could no longer be found. In contrast, ten min after replacing the MWCNT containing media with standard growth media, MWCNT-L and MWCNT-S fibers were not detached from the ciliated cells and could be observed associated with the cilia and/or cell surface (black arrows in Fig. 1A). In the cilia activity test, FMS did not reduce the percentage of cells with active cilia compared to the vehicle group (Fig. 1B). However, the percentage of cells with active cilia in the MWCNT-L treated group was significantly reduced (2.73 ± 1.37; n = 3, $p < 0.05$) compared to the vehicle (18.7 ± 4.28) and FMS (16.57 ± 0.65) groups after 12 hr. Although not significant, a similar decrease was also observed in the MWCNT-S group.

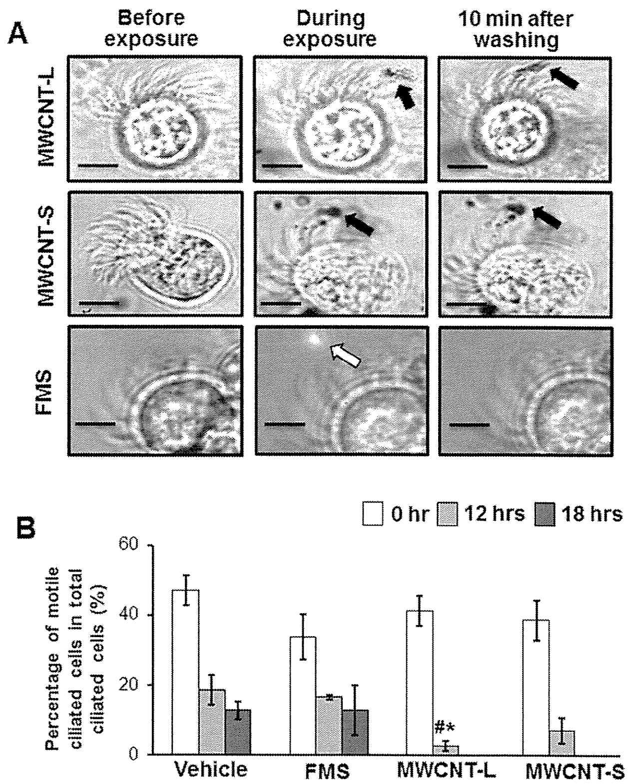

Fig. 1. Exposure of MWCNT to isolated tracheal ciliated cells *in vitro*. A, Images of ciliated cells exposed to fluorescent microsphere (FMS), MWCNT-L, and MWCNT-S; left, before exposure; middle, during exposure; right, after media change. FMS (white arrow) was clearly removed. MWCNTs were not removed (black arrows). Bars equal 5 µm. B, Percentage of cells with active cilia at time 0 and 12 and 18 hr after media change. n = 3; * $p < 0.05$ vs vehicle control, # $p < 0.05$ vs FMS control.

Rat study

The majority of the epithelium of the trachea is com-